# Copyright Warning & Restrictions

The copyright law of the United States (Title 17, United States Code) governs the making of photocopies or other reproductions of copyrighted material.

Under certain conditions specified in the law, libraries and archives are authorized to furnish a photocopy or other reproduction. One of these specified conditions is that the photocopy or reproduction is not to be "used for any purpose other than private study, scholarship, or research." If a, user makes a request for, or later uses, a photocopy or reproduction for purposes in excess of "fair use" that user may be liable for copyright infringement,

This institution reserves the right to refuse to accept a copying order if, in its judgment, fulfillment of the order would involve violation of copyright law.

Please Note: The author retains the copyright while the New Jersey Institute of Technology reserves the right to distribute this thesis or dissertation

Printing note: If you do not wish to print this page, then select "Pages from: first page # to: last page #" on the print dialog screen

## ABSTRACT

### DEVELOPMENT OF FLEXIBLE BATTERIES USING NANO-CARBONS AND POLYMERS

**by**
**Zhiqian Wang**

Flexible electronics such as wearable equipment, displays, cell phones and smart cards require flexible power sources like batteries. In this thesis, the development of flexible batteries and supercapacitors are presented. Different types of flexible batteries including zinc carbon batteries, primary alkaline batteries, secondary alkaline batteries and zinc air cells are presented, These were designed, fabricated and improved using polymers and nano-carbons like carbon nanotubes (CNTs). CNTs are found to be effective as conductive additives compared to the traditional graphite. Purification is important to remove impurities that lead to side reactions/ corrosions. However, further treatment like carboxylation lead to higher electric resistance caused by the defects on CNT surface, which are created during the CNT acid treatment and functionalization. In case of secondary alkaline cells, CNTs can also provide channel for electrolyte to facilitate the recharge process.

Throughout the research in developing flexible batteries, it is found that polymers like polyethylene oxide (PEO) are used as binders to maintain flexibility; poly(3,4-ethylenedioxythiophene)-poly(styrenesulfonate) (PEDOT:PSS) to be an effective conductive additive in acidic/neutral conditions; polyvinyl alcohol (PVA)-poly (acrylic acid) (PAA) copolymer separator membrane is found to be an effective separator and electrolyte storage in alkaline electrolyte.

Efforts are also made to generate highly defective and oxidized CNTs for fabrication of supercapacitor electrodes is also presented. CNTs are treated under microwave conditions for different durations to generate varying amounts of defects and oxidation levels. This is evidenced by the increase in BET surface area, D to G ratio and oxygen content with increase in treatment time. Under the given conditions, a treatment time of 40 min is found to be optimum, beyond which the increase in any of these properties as well as in specific capacitance is minimal. The increase in surface area enhances the double layer capacitance while the oxygenation may lead to pseudocapacitance. Together these make microwave treatment of CNTs an attractive approach to enhance supercapacitor performance.

# DEVELOPMENT OF FLEXIBLE BATTERIES USING NANO-CARBONS AND POLYMERS

**by**
**Zhiqian Wang**

**A Dissertation**
**Submitted to the Faculty of**
**New Jersey Institute of Technology**
**in Partial Fulfillment of the Requirements for the Degree of**
**Doctor of Philosophy in Chemistry**

**Department of Chemistry and Environmental Science**

**May 2015**

.

**APPROVAL PAGE**

**DEVELOPMENT OF FLEXIBLE BATTERIES USING NANO-CARBONS AND POLYMERS**

**Zhiqian Wang**

---

Dr. Somenath Mitra, Dissertation Advisor — Date
Distinguished Professor of Chemistry and Environmental Science, NJIT

---

Dr. Edgardo Farinas, Committee Member — Date
Associate Professor and Chair of Chemistry and Environmental Science, NJIT

---

Dr. Tamara Gund, Committee Member — Date
Professor of Chemistry and Environmental Science, NJIT

---

Dr. Haidong Huang, Committee Member — Date
Assistant Professor of Chemistry and Environmental Science, NJIT

---

Dr. Pradyot Patnaik, Committee Member — Date
Consultant, Radiance

## BIOGRAPHICAL SKETCH

**Author:** Zhiqian Wang

**Degree:** Doctor of Philosophy

**Date:** May 2015

**Undergraduate and Graduate Education:**

- Doctor of Philosophy in Chemistry,
  New Jersey Institute of Technology, Newark, NJ, 2015

- Bachelor of Engineering in Applied Chemistry,
  China University of Mining and Technology (Beijing), Beijing, P. R. China, 2008

**Major:** Chemistry

**Presentations and Publications:**

Z. Wang, N. Bramnik, S. Roy, G. D. Benedetto, J. L. Zunino III, S. Mitra, "Flexible zinc-carbon batteries with multiwalled carbon nanotube/conductive polymer cathode matrix", Journal of Power Sources 237 (2013) 210-214.

Z. Wang, Z. Wu, N. Bramnik, S. Mitra, "Fabrication of high performance flexible alkaline batteries by implementing multi-walled carbon nanotubes and copolymer separator", Advanced Materials 26 (2014) 970-976.

Z. Wang, S. Mitra, "Development of flexible secondary alkaline battery with carbon nanotube enhanced electrodes", Journal of Power Sources 266 (2014) 296-303.

Z. Wang, Z. Wu, G. D. Benedetto, J. L. Zunino III, S. Mitra, "Microwave Synthesis of Highly Oxidized and Defective Carbon Nanotubes for Enhancing the Performance of Supercapacitors", Carbon (2015) *doi: 10.1016/j.carbon.2015.04.045*

X. C. Lau, Z. Wang, S. Mitra, "A C70-carbon nanotube complex for bulk heterojunction photovoltaic cells", Appl. Phys. Lett. 103 (2013) 243108.

X. C. Lau, Z. Wang, S. Mitra, "Effect of low concentrations of carbon clack in organic solar cells", Solar Energy Materials and Solar Cells 128 (2014) 69-76.

Z. Wu, R. F. Hamilton Jr., Z. Wang, A. Holian, S. Mitra, “Oxidation debris in microwave functionalized carbon nanotubes: chemical and biological effects”, Carbon 68 (2014) 678-686.

S. Mitra, Z. Wang, “Flexible alkaline battery”, US patent Application: US 20140199578 A1.

Z. Wang, Z. Wu, N. Bramnik, S. Mitra "Development of flexible alkaline batteries with carbon nanotube and polymers”, American Chemical Society 249th ACS National Meeting, Denver, CO, March 25, 2015.

Z. Wang, G. D. Benedetto, J. L. Zunino III, S. Mitra, "Platform technology for the development of flexible batteries with composite carbon nanotube electrodes”, American Chemical Society 249th ACS National Meeting, Denver, CO, March 24, 2015.

Z. Wang, S. Mitra, “Flexible Battery – a conformal power source that is a promising alternative to traditional AA/AAA batteries”, NJEN New Jersey Entrepreneurial Network Event, Princeton, NJ, February 2014.

Z. Wang, S. Mitra, “Flexible Zn/$MnO_2$ batteries with nanostructured electrodes”, NERM 2012 American Chemical Society 38th Northeast Regional Meeting, Rochester, NY, October 2012.

There is still a long way to go and much work to do. The diploma is only another beginning.

奋斗 X 多年，拿到 N 张纸。仍然任重而道远。

## ACKNOWLEDGMENT

I would like to thank my thesis advisor, Dr. Somenath Mitra for his guidance and help during my doctoral studies. He helped to build up my logical thinking and improve my skills of writing. I am grateful to my committee members: Dr. Edgardo Farinas; Dr. Tamara Gund; Dr. Haidong Huang; Dr. Pradyot Patnaik for their advices and support.

Specially, I would thank U.S. Army for their funding and technical support during my studies; also the Department of Chemistry and Environmental Science for their financial assistantship and instrument.

I would also thank Mr. Yogesh Gandhi, Dr. Yong Pu for technical and equipment support as well as other fellows including Dr. Natalia Bramnik and Zheqiong Wu who had been working together with me on my research project and provided helpful suggestions.

Finally, I would thank my family and friends who have been behind me for all these years.

## TABLE OF CONTENTS

**TABLE OF CONTENTS**
**(Continued)**

**Chapter** **Page**

## LIST OF TABLES

## LIST OF FIGURES

## LIST OF FIGURES
## (Continued)

# CHAPTER 1

# INTRODUCTION

## 1.1 Batteries and Capacitors

A battery is a device that converts its chemical energy into electric energy by electrochemical redox reactions. A battery is composed of one or multiple cells, when a cell is a basic electrochemical unit composed of electrodes (cathode/ positive electrode and anode/ negative electrode), separator, electrolytes, current collectors and container. During the discharge process, the anode gives up electrons to external circuit and is oxidized; the cathode gains electrons via external circuit and gets reduced. Batteries, either disposable or rechargeable, differ from reserve batteries and fuel cells that they are readily assembled: in a reserve battery one key component is separated from other parts of the battery; and hence, the battery is subject to activation prior to any usage; fuels cells require active materials from external sources to be fed into the cells.

For a cell with redox reaction shown in the below equations:

$$aA + bB \rightarrow cC + dD \quad \text{(overall)}$$

$$aA + ne^- \rightarrow cC \quad \text{(cathode)}$$

$$bB \rightarrow ne^- + dD \quad \text{(anode)}$$

the voltage E is given by Nernst equation:

$$E = E_0 - \frac{RT}{nF} ln \frac{Ca^c Da^d}{Aa^a Ba^b}$$

where $E_0$ is the standard electromotive force, $i_a$ is the activity of species, R is the gas constant, T is the temperature, F is Faraday constant, n is the electrons transferred in the reaction. Hence, in a certain system, the changes in species activity (concentration, surface

area) can slightly increase the output voltage of a battery cell. Besides, the faster the reaction can happen, the higher power a cell can deliver. Other factors affecting battery performance include temperature, internal resistance, chemical deterioration of electrochemical materials and mode of discharge.

Zinc has been the most popular anode material, especially in primary batteries, for its good electrochemical behavior, low cost and availability; Aluminum is also attractive for its electrochemical potential and abundance; lithium provides high energy density and power density, though requires non-aqueous electrolytes in most cases. Most common types of batteries include zinc-carbon batteries available as D, AA and AAA batteries; alkaline batteries in the form of AA, AAA, 9V batteries; lead acid batteries as car batteries; Ni-MH batteries also as rechargeable AA, AAA batteries; lithium ion batteries in cell phones and laptop computers; zinc air and zinc silver batteries as button cells.

Zinc carbon batteries, using zinc anodes (cylinder) and $MnO_2$ cathodes, are reliable low-cost primary batteries often used in flashlights, remote controls, toys and portable radios. In 1866 the first prototype of modern dry cell was developed. In the $20^{th}$ century the zinc carbon batteries gradually evolve, with improved $MnO_2$ and electrolytes. Specially, in the 1960s, zinc chloride cells were developed, improving heavy duty performance. The chemical reactions are as follows:

$$Zn + 2MnO_2 + 2NH_4Cl \rightarrow 2MnOOH + Zn(NH_3)_2Cl_2 \qquad \text{(Leclanché)}$$

$$Zn + 2MnO_2 + 2ZnCl_2 + 2H_2O \rightarrow 2MnOOH + 2Zn(OH)Cl \qquad \text{(zinc chloride)}$$

Alkaline batteries using zinc anodes and $MnO_2$ cathodes but alkaline electrolytes were first commercially introduced in 1959. They have been taking the market share of zinc carbon batteries due to better performance and low temperature performance. The

costs of these batteries are still relatively low compared to lithium systems. Unlike zinc carbon batteries, alkaline batteries use powdered zinc in anode, with alloying elements to control gassing. The reactions are as follows:

$$Zn + 2MnO_2 + 2H_2O \rightarrow 2MnOOH + Zn(OH)_2$$

$$Zn(OH)_2 \rightarrow ZnO + H_2O$$

Some alkaline batteries are designed to be rechargeable, with compositions similar to primary alkaline batteries; the electrochemical reactions are reversed during the charge process. However, additives are required to acquire the rechargeability: bismuth are required to prevent the soluble manganese species migrate from cathode to zinc anode. Besides, separators that can prevent internal short circuit due to zinc dendrite are necessary. Cycle life of a rechargeable alkaline battery is short, with the capacity fades after cycles. They are more suitable for less deep discharges, and should be charged after partially discharge to maintain the capacity better.

A zinc air battery consists of a zinc anode, alkaline electrolyte and a cathode with catalysts. Air/ oxygen is allowed into the cathode. Using oxygen in the air as cathode active material, the energy density for zinc air battery is high. The electrochemical reaction is as follow:

$$2Zn + O_2 \rightarrow 2ZnO$$

Yet due to the low concentration of oxygen, the power is low. These cells are also more sensitive to environmental factors such as moisture, carbon dioxide concentration and temperature. They are also not suitable for intermittent uses.

Batteries provide electricity via electrochemical redox reactions between cathodes and anodes. However, due to the limitation of reaction rates, needs for output power can

hardly be meet in many cases. Electrochemical capacitors, which store energy by charge separation, are developed as alternatives to batteries. Like a battery cell, a electrochemical capacitor/ supercapacitor also has two electrodes immersed in electrolyte with a separator between them. There are two basic mechanisms how an electrochemical capacitor works: double-layer capacitance and pseudocapacitance. In the former mechanism charge is stored electrostatically, or non-Faradaically, and there is no transfer of charge between electrode and electrolyte. There are no chemical or composition changes associated with non-Faradaic processes either. Since the double layer effect takes place at the boundary of the electrode-electrolyte phase, the available surface area plays an important role. In pseudocapacitance, charge is transferred between electrode materials and electrolyte, with electrosorption, reduction-oxidation reactions, and intercalation processes. Many metal oxides like $RuO_2$ have shown large specific capacitance.

## 1.2 Flexible Power Sources

The increasing interest to flexible/portable electronics requires the development of flexible power sources like flexible batteries, which can be implemented in products such as smart cards, flexible displays, memory chips, smart watch belts as well as pharmaceutical and cosmetic transdermal delivery patches. The flexible power sources can also be combined with energy harvest devices, such as window shades with solar cell on one side and batteries on the other. These flexible batteries can be manufactured by commercially available cost-effective printing techniques like screen printing.

Research has been focused on the development of different aspects of the flexible battery manufacturing processes, including design of the cells, current collectors, electrodes ink as well as electrolyte formulations. Just like traditional batteries, one battery

is composed of one or multiple electrochemical cells, when each cell is composed of anode, cathode, separator, electrolyte and in most cases current collectors on both electrodes. The basic design of a single-cell flexible pouch battery is shown in Figure 1.1. Each component of the cell has to be flexible.

Different types of flexible power sources including batteries and capacitors are being developed, like zinc-$MnO_2$ batteries (P. Hiralal, S. Imaizumi et al., 2010) (A. M. Gaikwad, G. L. Whiting et al., 2011), lithium-ion batteries (L. Hu, H. Wu et al., 2010) (X. Jia, C. Yan et al., 2011). Batteries are even fabricated on textiles to serve as wearable electronics (L. Bao and X. Li, 2012). Generally, the aqueous battery systems are safer and have lower costs, more friendly to the environment, though their performance tend to be lower; while the ones with organic electrolyte like lithium-ion batteries provide higher performance.

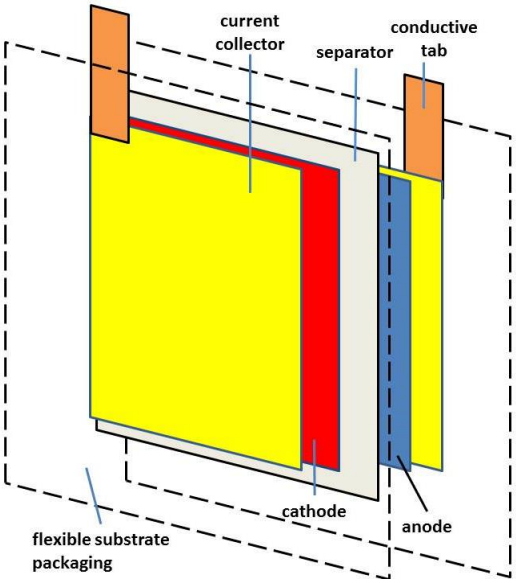


**Figure 1.1** Basic design of a flexible pouch battery.
*Source: Z. Wang, S. Mitra 2014*

### 1.3 Nano-carbons and their Treatment

Due to their high electrical conductivity and large surface area, carbon nanotubes (CNTs) have attracted much attention as effective conductive additives in aqueous cells (P. Hiralal, S. Imaizumi et al., 2010), or active electrode materials for composite electrodes in electrochemical energy storage devices such as lithium ion batteries (L. Hu, H. Wu et al., 2010) (X. Jia, C. Yan et al., 2011), and supercapacitors (R. K. Sharma and L. Zhai, 2009). On the other hand, the extraordinary mechanical properties, including high strength and flexibility, make CNTs a very promising component for thin and flexible electrodes. In many studies, singlewalled carbon nanotubes (SWCNTs) have been utilized as conductive additives in non-Li batteries, primarily as conductive additives or current collectors. However, these SWCNTs are more expensive than their multiwalled counter parts: the multiwalled carbon nanotubes (MWCNTs). Besides, similar to carbon fibers, the CNTs can also serve as the matrix or scaffolds for active materials.

There have been efforts to improve the performance of CNTs via functionalization to add functional groups and generating defects via conventional chemical techniques such as acid treatment, refluxing and sonication (C. G. Salzmann et al., 2007), (F. Hauke et al., 2010; A. Stein et al., 2009) and (W. Huang et al., 2002). Hence, functional groups like hydrophilic carboxylic groups can be generated, changing many characteristics including the dispersibility in water, conductivity and redox properties. However, those reactions are mostly both energy and time-consuming. Microwave treatment of CNTs is known to cause in-situ super heating leading to fast reactions with high degree of functionalization (Y. Wang et al., 2005) (Y. Chen et al., 2008). Such treatment of CNTs can also be used to remove impurities like metal and metal oxides in the CNTs. The purification of CNTs was

carried out in the microwave accelerated reaction system by dispersing pre-weighed CNTs into dilute $HNO_3$. The reaction vessels were subject to microwave radiation at a preset temperature for several minutes. The carboxylated functionalization/ destruction of CNTs were generally carried out in the microwave accelerated reaction system by dispersing pre-weighed CNTs into a mixture of concentrated $H_2SO_4$ and $HNO_3$ and treated at higher preset temperatures for longer time. After cooling down to room temperature, the CNT products were vacuum filtered and washed using Milli Q water through until neutral. Samples were then finally dried in the vacuum oven until a constant weight was achieved.

# CHAPTER 2

# FLEXIBLE ZINC-CARBON BATTERIES

In Chapter 2, flexible zinc-carbon batteries were designed, fabricated and optimized. Multiwalled carbon nanotubes (MWCNTs) and conductive polymer poly(3,4-ethylenedioxythiophene)-poly(styrenesulfonate) (PEDOT:PSS) were implemented for the development of highly conductive composite electrode for flexible batteries.

## 2.1 Zinc-Carbon Cells

Zinc-carbon batteries are among the earliest commercially available consumer batteries. From the earlier Leclanché cells to the later zinc chloride cells, they used zinc as anode active material, $MnO_2$ as cathode material and neutral or weak acidic electrolyte line $ZnCl_2$. These zinc-carbon batteries feature lower costs and safety due to water-based electrolytes as well as inexpensive and environmentally friendly electrode materials. The production costs of zinc-carbon cells are relatively low due to water-based electrolyte as well as inexpensive and environmentally friendly electrode materials.

It is known that $MnO_2$ is a poor electrical conductor, so conductive additives (usually, graphite or carbon black) are added to cathode in zinc-carbon batteries. There is also the possibility of adding other conducting materials, like polymers, to enhance conductivity. For example, poly(3,4-ethylenedioxythiophene)-poly(styrenesulfonate) (PEDOT:PSS): PEDOT is known to be a stable conductive polymer which has been successfully applied as an electrode material for organic solar cells (Y. H. Kim et al., 2011) and capacitors (C. Lei et al., 2011) (A. Laforgue, 2011). Hence, it is believed that under

light acidic or neutral conditions, PEDOT:PSS could also serve as an effective conductive additive.

### 2.2 Flexible Zn-C Cell Fabrication

The cathode paste was prepared by mixing $MnO_2$ powder (Aldrich, ≥ 99.99%, trace metal basis), polyvinylpyrrolidone (PVP, Aldrich, average mol wt. 10000), 1.3% wt aqueous dispersion of poly(3,4-ethylenedioxythiophene)-poly(styrenesulfonate) (PEDOT:PSS, Aldrich) and MWCNTs (purity 95%, Cheap Tubes Inc. Brattleboro, VT, USA). After mixing the components, the aqueous paste was sonicated for at least 10 minutes using OMNI SONIC RUPTOR 250 ultrasonic homogenizer. For comparison, the cathode mixture with synthetic graphite (Aldrich, <20 micron) instead of MWCNTs was prepared as well. The MWCNTs used were as received or functionalized prior to the electrode preparation to improve their dispersibility in the solvent/electrode matrix. Typically, dry cathode contained 87.0% w/w $MnO_2$, 3% w/w PVP, and the rest being MWCNTs and sometimes PEDOT:PSS. The optimum $MnO_2$:MWCNTs ratio in the cathode mixture was to determine. The anode mixture for flexible batteries was made of zinc powder (Sigma Aldrich, ≤10 μm, ≥ 98%) mixed with PVP and PEDOT:PSS aqueous solution. The anode after drying contained 83.5% w/w Zn dust, 2% w/w PVP, rest being PEDOT:PSS and Zn acetate.

The flexible electrodes were prepared by casting the electrode slurry onto the carbon tape (NEM tape, Nisshin EMCO Ltd) current collector. Before casting, the carbon tape was stuck to the adhesive side of polyethylene terephthalate (PET) film coated with

ethylene vinyl acetate copolymer (EVA) resin. The typical electrode area was 4cm × 5cm. Copper foil strips stuck to the silver coated carbon tape served as electrode tabs.

The electrode slurries were applied onto the current collectors and dried at 50°C for 30 minutes. The last 5 minutes of drying was processed under vacuum (pressure 9.893 kPa, with atmosphere pressure 101 kPa) to remove all residual water. The typical weights of the dry cathode and anode were 0.5 and 1 g, respectively. The electrodes were assembled co-facially with the craft paper separator (MUNKSJÖ paper) in between, which had been previously soaked in saturated zinc acetate electrolyte. The electrolyte also contained 600 ppm lead chloride and 1000 ppm hexadecyltrimethylammonium bromide (HDTAB, Sigma Aldrich, ≥ 99%) as inhibitors. The batteries were then thermally sealed.

The cathode optimization was carried on in metal Swagelok cells with Zn-foil as anode. In this case, the cathode slurry was cast directly onto the stainless steel current collector (25 mm diameter) and dried. The typical weight of the cathode paste after drying was 0.1 g. For all cells, the Zn anode was taken in excess in respect to $MnO_2$ cathode.

Scanning electron microscope (SEM) images were collected on a LEO 1530 VP Scanning Electron Microscope. Electrode materials were cast onto flat surface and dried to form a 0.2 mm thick layer of 1 cm × 1 cm. The surface resistance between two ends of the above layer was measured using Keithley digital multimeter to compare the electrode conductivity. The batteries were discharged under constant resistance mode (2640 Ω) using MTI Battery Analyzer (Richmond, CA). Flexible batteries were also attached to a cylindrical substrates of different diameters to test the performance under bending conditions.

## 2.3 Optimization of Flexible Cells

**Table 2.1** Electrode Resistance of Zn-C Battery Cathodes with Different Formulations

| Sample | Surface resistance of 1 $cm^2$ area (KΩ) | Description of the sample |
|---|---|---|
| 1 | 3.26 | PVP/$MnO_2$/Graphite |
| 2 | 0.86 | PVP/PEDOT:PSS/$MnO_2$/Graphite |
| 3 | 0.37 | PVP/ PEDOT:PSS/$MnO_2$/CNTs (raw) |
| 4 | 0.54 | PVP/PEDOT:PSS/$MnO_2$/CNTs (functionalized) |

*Source: Z. Wang et al., 2013*

The surface resistance of the cathode composed of $MnO_2$, graphite and PVP was 3.26 KΩ (see Table 2.1). In addition, PEDOT:PSS was added to increase the overall conductivity of the $MnO_2$ cathode. The addition of 1% PEDOT:PSS significantly reduced the resistance of the cathode down to 0.86 KΩ. The internal resistance of the electrodes may have contributed to lowering the operation voltages compared to the theoretical value. The addition of PEDOT:PSS to our composite electrode (1% w/w) had a strong impact on the electrochemical performance (Figure 2.1). Besides being a conductive polymer (C. Ionescu-Zanetti, A. Mechler et al., 2004) (Z. Hu, J. Zhang et al., 2011) (Y. Kim, J. Lee et al., 2012), the PEDOT:PSS showed poor solubility in the electrolyte. It was inferred that it formed conductive layers and bind/ bridged particles together.

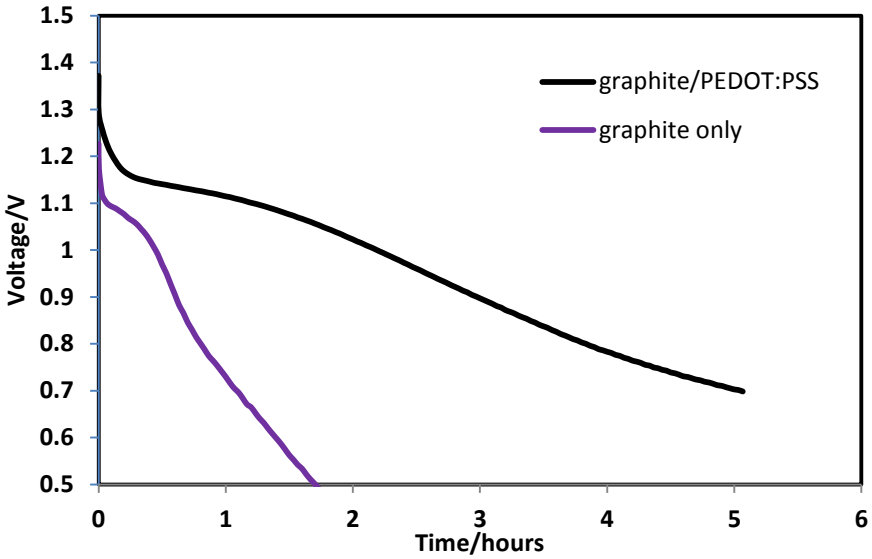


**Figure 2.1** Discharge curves of Zn-C cells with and without PEDOT: PSS. Graphite (8.6% w/w) was added as the conductive additive. The discharge was performed in constant resistance mode in a metal cell with Zn-foil anode and $Zn(CH_3COO)_2$ electrolyte.
*Source: Z. Wang et al., 2013*

As compared to graphite, the MWCNTs decreased the resistance of the cathode from 0.86 to 0.37 KΩ. This indicated that MWCNTs were more effective in creating the conductive network. The electrode prepared with functionalized MWCNTs demonstrated slightly higher resistance (0.54 KΩ) than the ones with raw MWCNTs. The hydrophilic carboxylation usually leads to improved wettability and dispersibility (T. W. Chou et al., 2010). Therefore, carboxylation might significantly enhance the electrical conductivity of CNT composites by promoting better interfacial interactions (Y. Liu, L. Gao, 2005), (Z. Spytalsky et al., 2005), (Q. Li et al., 2007). On the other hand, the covalent functionalization could also create large numbers of defects on the CNT surface and decrease electron mobility and conductivity. In this case, it appeared that the improvement in dispersibility did not outweigh the increase in resistivity. The SEM images confirmed this assumption [Figure 2.2 (a), (b)] where relatively homogeneous distribution of both raw and functionalized MWCNTs was observed in the composite cathodes. No significant

enhancement of the homogeneity was observed after carboxylation of MWCNTs. Therefore, in this case, the functionalization did not improve electrode performance.

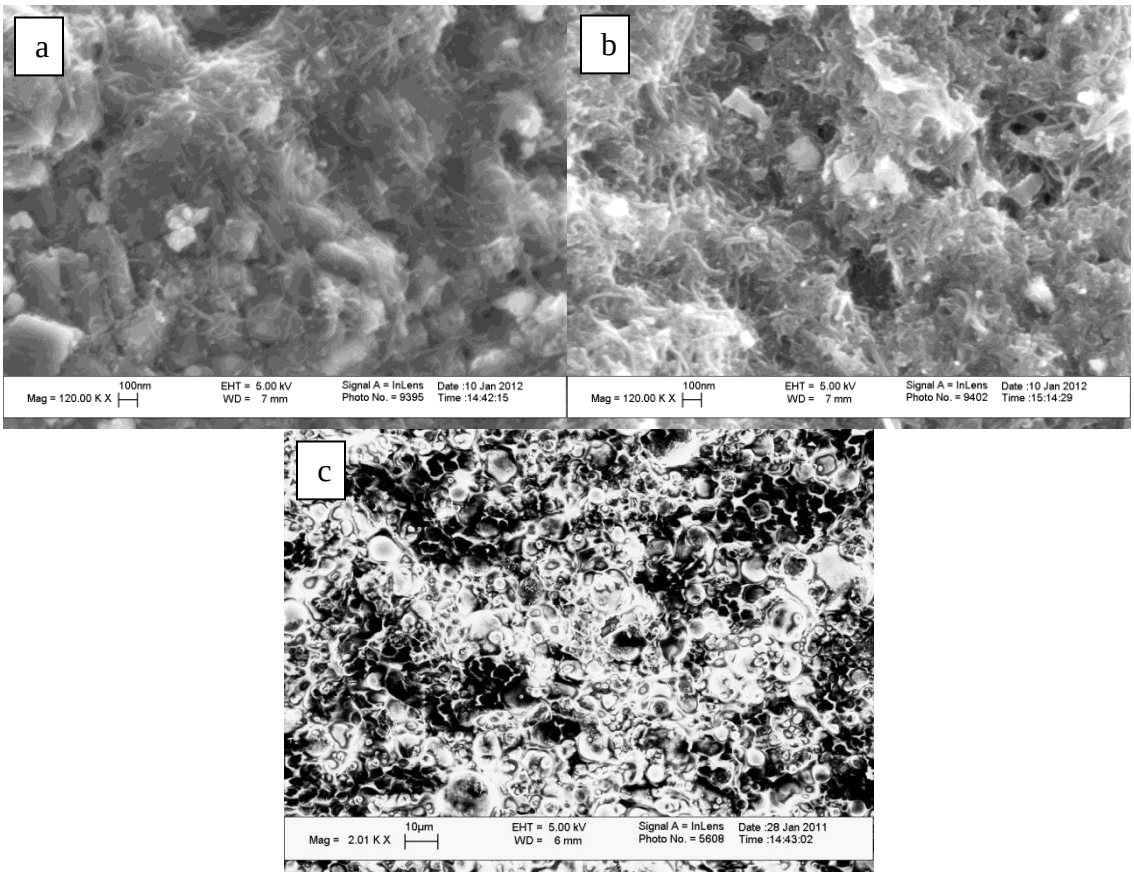


**Figure 2.2** SEM images of Zn-C cell composite electrodes: (a) $MnO_2$-cathode (8.6% raw MWCNTs as conductive additive); (b) $MnO_2$-cathode (8.6% w/w functionalized MWCNTs as conductive additive); (c) anode made of micron size Zn particles.
*Source: Z. Wang et al., 2013*

The electrochemical performance of $MnO_2$ cathodes prepared with 1% PEDOT:PSS and different carbon conductive additives, namely, graphite, raw MWCNTs and COOH-functionalized MWCNTs (Figure 2.3) were measured. Upon discharge down to 0.7 V, the cathode with raw MWCNTs exhibited the highest operation voltage and longest operation time (see Figure 2.3). The superior performance of raw MWCNTs compared to the graphite is in good agreement with the results of the resistance

measurements. The presence of the conductive additive and the more efficient network of the MWCNTs resulted in higher conductivity and a higher discharge voltage. Increasing the concentration of raw MWCNTs resulted in the higher operation voltage and higher discharge capacity. This is seen from Figure 2.4. Performance data of different cells are listed in Table 2.2, which shows that increasing the concentration of CNTs enhanced battery performance. The specific capacity obtained for the cathode with 8.6% graphite to 12% MWCNTs increased from 4.5 to 120 mAh $g^{-1}$. The corresponding $MnO_2$ utilization for the graphite and the MWNT system increased from 1.5 to 39% of the theoretical value of 308 mAh $g^{-1}$ $MnO_2$. This value is in line with what has been reported before with SWCNTs. It should be noted that a different discharge mode was used in that study.

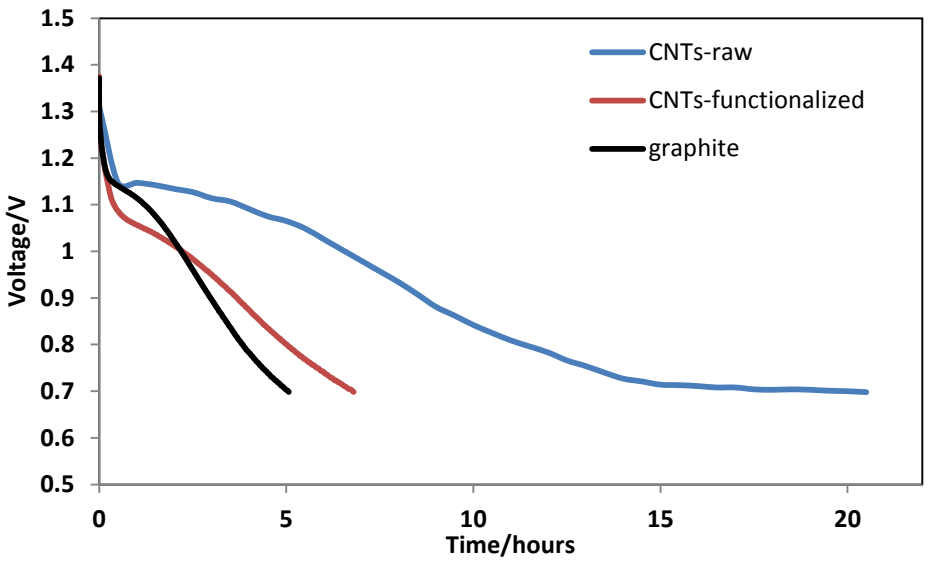


**Figure 2.3** Discharge of curves Zn-C cells with different carbons (8.6% w/w). The discharges was performed in constant resistance mode in a metal cell with Zn-foil anode and $Zn(CH_3COO)_2$ electrolyte.
*Source: Z. Wang et al., 2013*

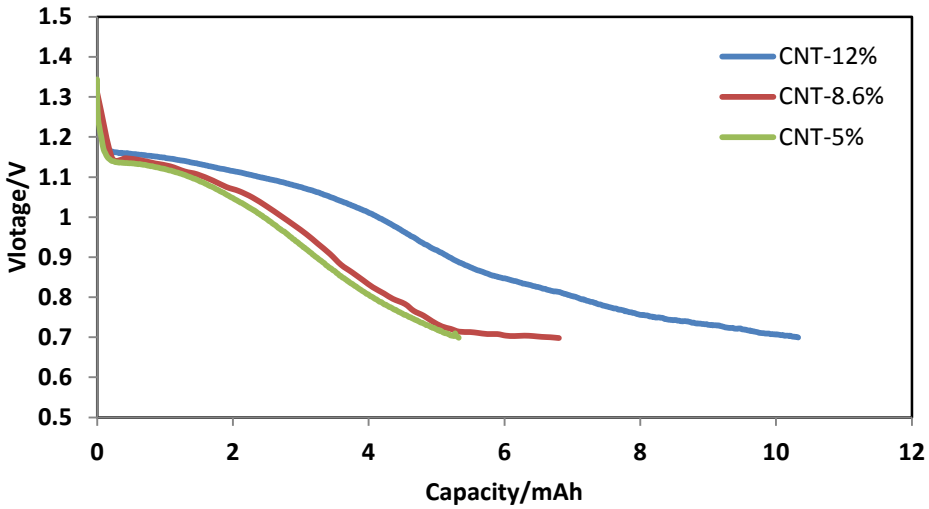


**Figure 2.4** Voltage-capacity curves for Zn-C cells with raw CNTs in cathode. The discharge was performed in constant resistance mode in a metal cell with Zn-foil anode and $Zn(CH_3COO)_2$ electrolyte.
*Source: Z. Wang et al., 2013*

**Table 2.2** Specific performance data of different cells (in metal cells)

| Description of the Cell | Specific Capacity (mAh $g^{-1}$ $MnO_2$) | Specific Energy (mWh $g^{-1}$ $MnO_2$) | $MnO_2$ Utilization (%) |
|---|---|---|---|
| $MnO_2$/Graphite | 4.50 | 4.27 | 1.5 |
| $MnO_2$/Graphite/ PEDOT:PSS | 21.0 | 20.4 | 6.82 |
| PVP/PEDOT:PSS/ $MnO_2$/CNTs (8.6%, raw) | 77.3 | 71.0 | 25.1 |
| PVP/PEDOT:PSS/ $MnO_2$/CNTs (8.6%, functionalized) | 27.1 | 25.4 | 8.80 |
| PVP/PEDOT:PSS/ $MnO_2$/CNTs (5%, raw) | 61.5 | 58.7 | 20.0 |
| PVP/PEDOT:PSS/ $MnO_2$/CNTs (12%, raw) | 120 | 111 | 39.0 |

*Source: Z. Wang et al., 2013*

Anode made of micron size zinc powder [Figure 2.2 (c)] not only showed higher flexibility than zinc foil, but also had greater surface area facilitating a faster reaction. However, anodes with zinc nanoparticles showed significant corrosion and the batteries failed rather quickly. It is possible that the nanoparticles enhanced the gassing side reaction, generating hydrogen. Consequently, particle size of the zinc powder was an important factor.

The flexible battery prepared with composite cathode and Zn-powder anode is shown in Figure 2.5. Upon discharge at a constant resistance of 2640 Ω, the flexible battery delivered about 15mAh capacity before significant voltage drop occurred. Typically, bending of the flexible battery can induce a compression of the cell stacking enhancing inter-particle contact and can also vary the contact adhesion between the electrodes and the separator. Bending may also result in cracking in some areas due to the stress on the composite especially in the case of $MnO_2$. These factors are known to cause variation in performance. Testing the batteries under bending conditions revealed that for the most part the batteries retained their function, though there were some relatively small fluctuations and alterations in the performance. This is presented in Figure 2.6. In our opinion, the bending performance can be further improved by further optimization of the electrode composition, improving its mechanical properties and packaging process, and by the utilization of more conductive current collectors.

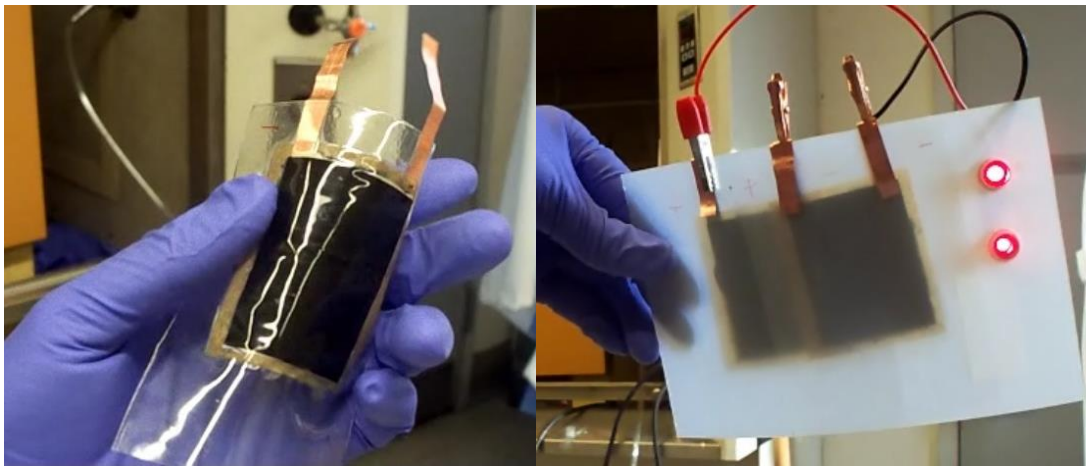

**Figure 2.5** Photograph of the flexible battery and LEDs powered by the flexible batteries.
*Source: Z. Wang et al., 2013*

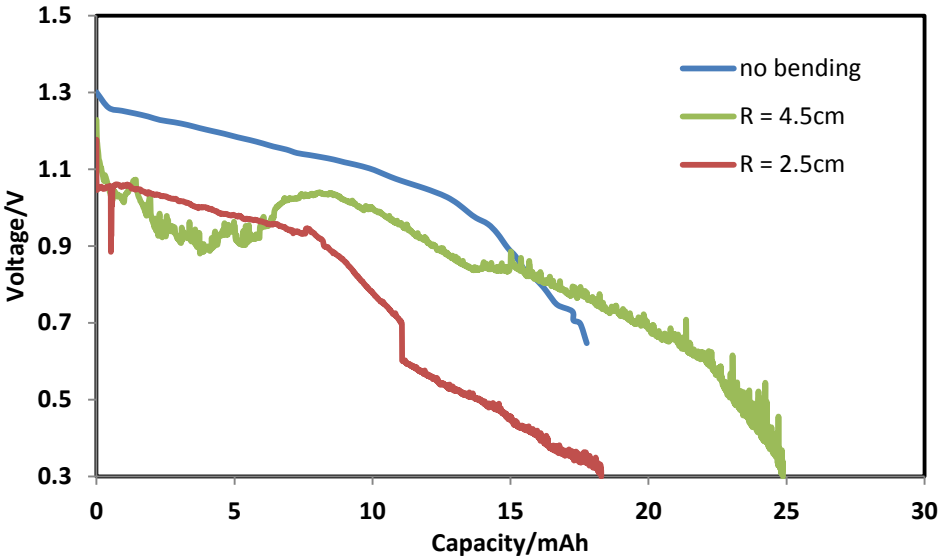


**Figure 2.6** Voltage-capacity curves for flexible Zn-C cells under bending conditions.
*Source: Z. Wang et al., 2013*

We have demonstrated a new approach to the fabrication of $MnO_2$ composite cathodes based on simultaneous use of conductive polymer PEDOT:PSS and MWCNTs as conductive additives. MWCNTs were found to be more effective in creating conductive networks compared to graphite. The oxidative functionalization of CNTs prior to the cathode fabrication appeared to increase the resistance of the electrode composite and to decrease the electrochemical performance. The relatively inexpensive raw MWCNTs

represent an advantageous alternative to significantly more expensive SWCNTs or less effective graphite in composite $MnO_2$ cathode.

# CHAPTER 3

# FLEXIBLE PRIMARY ALKALINE BATTERIES

## 3.1 Alkaline Batteries

Compared to lithium ion batteries, advantages of primary batteries with aqueous electrolytes include their eco-friendliness and ease of fabrication. Like zinc carbon cells, an alkaline battery uses $MnO_2$ as the cathode active material along with zinc as anode active material. The electrodes are soaked in alkaline electrolyte like KOH with a separator often made from a fibrous material such as cellulose or synthetic fibers. The alkaline batteries have been replacing zinc-carbon batteries for their higher durability especially under heavy load. However, reports on flexible alkaline cells are relatively few.

A flexible alkaline cell offers several challenges such as electrode flexibility, low internal resistance, gassing inhibition, and the retention of the electrolyte in the flexible cells. Each battery component need to be flexible and stable in the strong alkaline media. Particularly, the separator in a flexible alkaline cell is a key component that needs to be strong and stable enough to endure the high pH environment while maintaining its flexibility. Although they take up more space, polymer gel electrolyte/ separator using nylon mesh as scaffolds has been reported (A. M. Gaikwad et al., 2011). Free-standing films are preferred both as electrodes and separator so that more space can be reserved for the active material and the electrolyte. Polymer films with high ionic conductivity and flexibility are promising for battery fabrications. Both polyvinyl alcohol (PVA) and poly (acrylic acid) (PAA) have been reported as part of either polymer electrolyte or separator in flexible batteries (J. C. Bailey et al., 2010), (A. M. Gaikwad et al., 2011). PVA is known to be stable in alkaline environment, and a PVA-KOH-water system has been reported to

remain stable for a period of 2 years (A. A. Mohamad et al., 2003). The addition of PAA further increased the ionic conductivity (G. M. Wu et al., 2006). Another advantage of these polymers is that they can also hold electrolyte while maintaining flexibility. While the synthesis of PVA-PAA copolymers have been reported (G. M. Wu et al., 2006), (K. Kumeta et al., 2003) and (H. H. Wang et al., 1999), they are yet to be used as separator for flexible batteries. Besides, like zinc-carbon batteries, electrode resistance is another problem.

The objective of this chapter is to develop high performance, flexible alkaline battery with MWCNT electrode that shows high active material utilization. Yet another objective is to develop copolymer separators to maintain the flexibility.

## 3.2 Fabrication Methods

The cathode paste was prepared by mixing electrolytic manganese dioxide powder (EMD, TRONOX, ≥ 92%, AB Grade), polyethylene oxide (PEO, Sigma Aldrich, Mv~400,000) and conductive additives. Multiwalled carbon nanotubes (MWCNTs, purity 95%, diameter 20-30 nm, length 10-30 μm, Cheap Tubes Inc. Brattleboro, VT, USA) were used as received, purified or functionalized prior to the electrode preparation. Synthetic graphite (Sigma Aldrich, <20 micron) was used without further treatment. The purification and functionalization of CNTs was performed in a Microwave Accelerated Reaction System (Mode: CEM Mars) with acid treatment (Y. Chen, Z. Iqbal and S. Mitra, 2007) (Y. Chen, S. Mitra, 2008).

The powders were mixed and then added into DI water which served as the solvent. The slurry was mixed for at least 30 min, followed by 30 min sonication using OMNI

SONIC RUPTOR 250 ultrasonic homogenizer. Then the cathode slurry was stirred again for 20 hours to form a homogeneous cathode material. The cathode dry formulation in a flexible alkaline battery contained conductive additive (3 - 15%, w/w) and PEO binder (10%, w/w), with the rest being EMD. Cathode optimization was carried out with an anode that contained zinc (96%, w/w), ZnO (2%, w/w) and PEO (2%, w/w).

The anode paste was prepared by mixing zinc powder (Sigma Aldrich, ≤10 μm, ≥ 98%), PEO as binder, zinc oxide powder (Sigma Aldrich, ≥ 99%) and Bismuth (III) oxide (Sigma Aldrich, 90-210 nm particle size, ≥ 99.8%) inhibitors, and conductive additive. The powders were mixed in the presence of DI water, and then stirred to form a homogeneous anode paste. The anode dry formulation in a flexible alkaline battery contains ZnO (2%, w/w), conductive additive (0 - 2%, w/w), $Bi_2O_3$ (0 - 3%, w/w), PEO (2 - 8%, w/w) and the rest was zinc powder. In cases of anode optimization, cathode formulation was fixed as EMD (84%, w/w), graphite (6%, w/w) and PEO binder (10%, w/w). Scanning electron microscope (SEM) images were collected on the LEO 1530 VP Scanning Electron Microscope. Electrode materials were cast onto flat surface and dried to form a 0.2 mm thick layer with a 1 cm × 1 cm area. The resistance between two ends of the layer was measured using Keithley digital multi meter.

A copolymer film made from polyvinyl alcohol (PVA, Mowiol 18-88, Sigma Aldrich, Mv~130,000) and poly (acrylic acid) (PAA, Sigma Aldrich, Mv~450,000) was used as the separator in the flexible battery. PAA was first dissolved in 0.26% KOH solution, with mass ratio 1: 30, and stirred under 80 °C till all the solids dissolved. After a sonication for 30min, extra DI water was added along with PVA. The typical PVA:PAA mass ratio here was 2:1 to get a good balance between ionic conductivity and mechanical

strength (G. M. Wu et al., 2006). The solution was stirred at 70 °C till all the PVA dissolved. After another 30 min of sonication, the solution was again stirred for another 12 hours and allowed to settle for an additional 12 hours to remove air bubbles. The fluid was then cast onto a flat smooth surface and dried. After drying, the copolymer film was peeled from the surface and heated at 150 ~ 160 °C for 50 min for crosslinking by ester linkage (K. Kumeta et al., 2003). Typical thickness of such a copolymer film was 0.2mm. The Fourier transform infrared spectroscopy (FTIR) of the separator film was done on a Perkin-Elmer instrument (Waltham, MA).

After applying the electrode slurry onto the current collectors, the electrodes were allowed to dry at ~60°C for 30 minutes with the last 5 minutes under vacuum (9.893 kPa) to completely remove any residual water. For flexible cells the typical weights of the cathode and anode after drying were 0.315 and 0.64 g, respectively. The electrodes were assembled facing each other with the separator between them. Before assembling, the separator was soaked in electrolyte solution, which was 9M KOH solution with ZnO (6%). The battery was thermally sealed in a laminator.

The electrochemical performances of different formulations were measured in fixed Swagelok-type cells. In this case, the electrode paste was cast directly onto the current collectors and dried. The typical weight of the cathode paste after drying was 0.03 g. For both fixed and flexible cells, the Zn anode was taken in excess in respect to $MnO_2$ cathode to maintain anode conductivity. Glass microfiber filters (Grade GF/A: 1.6 µm, Whatman) were used as separator in fixed Swagelok-type cells.

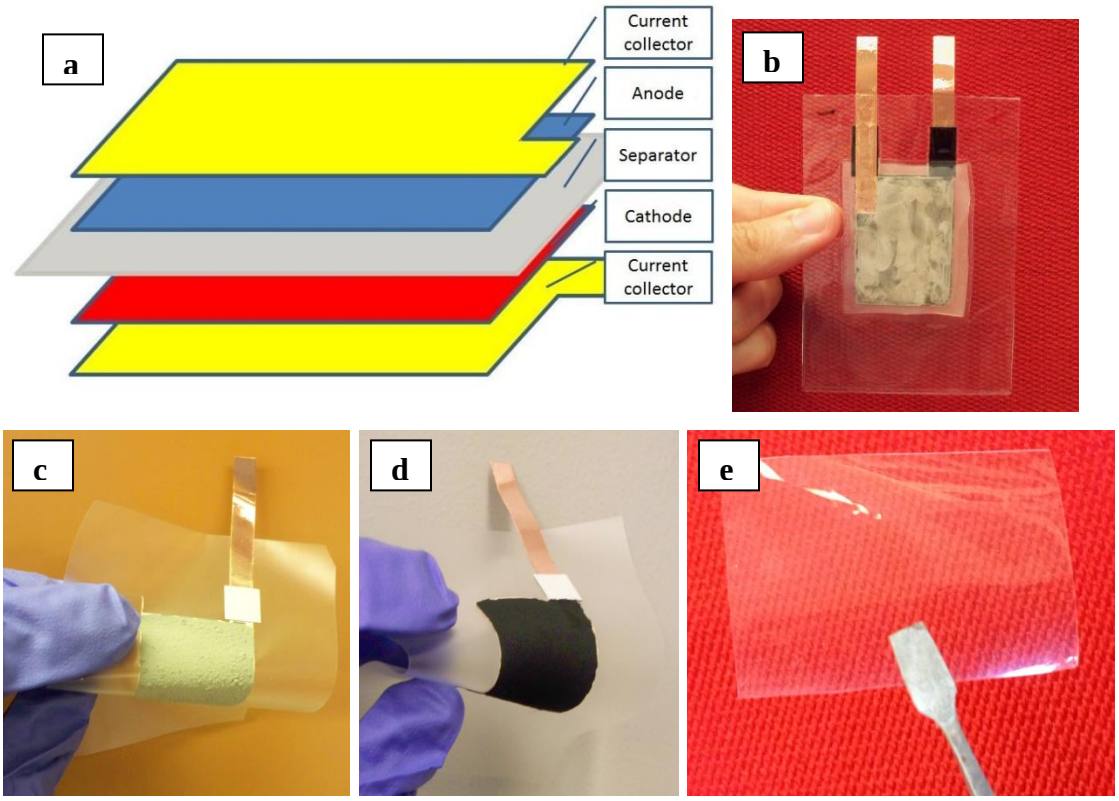


**Figure 3.1** Fabrication of flexible primary alkaline battery: (a) structure of a flexible cell; (b) assembled cell; (c) anode; (d) cathode; (e) PVA-PAA copolymer separator.
*Source: Z. Wang et al., 2014*

The flexible electrodes were prepared by casting the slurries onto the current collector made of silver ink (CAIG Laboratories Inc.) pasted directly onto the substrate. Batteries were fabricated in fixed metal cells while graphite rods (12.5 mm diameter) were used as current collectors. The flexible batteries were fabricated and encapsulated in polyethylene terephthalate (PET) film, which is coated with ethylene vinyl acetate copolymer (EVA) resin. The typical electrode area of a flexible battery was 3 cm × 4 cm. Copper foil strips stuck to the current collector served as electrode tabs. The bendable electrodes are shown in Figure 3.1.

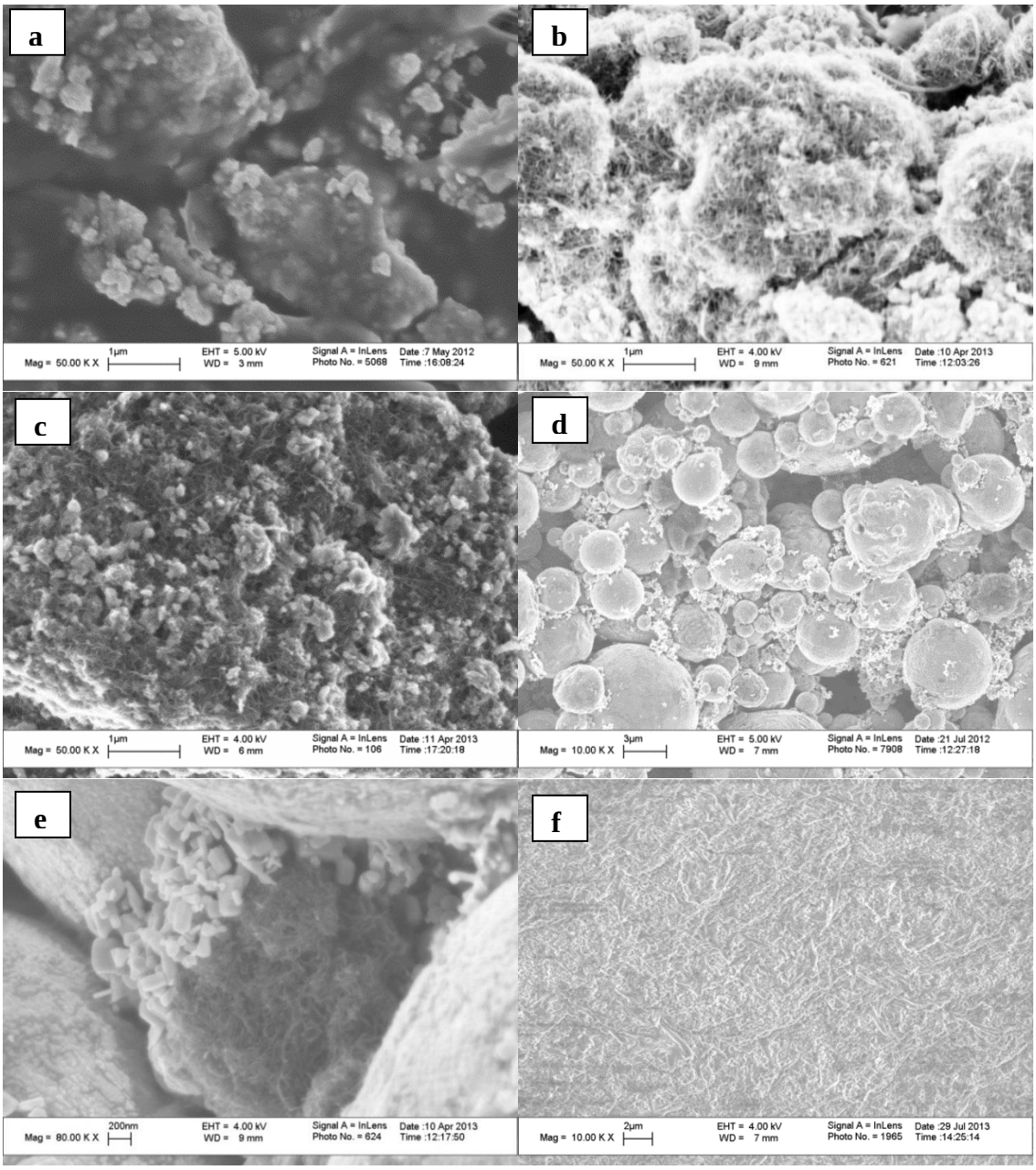


**Figure 3.2** SEM images of primary alkaline battery electrodes: (a) cathode with graphite; (b) cathode with purified CNTs; (c) cathode with CNT-COOH; (d) anode with micron size zinc particles; (e) CNTs among zinc particles in anode; (f) copolymer separator soaked in electrolyte.
*Source: Z. Wang et al., 2014*

The electrochemical performance of the battery was measured using MTI Battery Analyzer (Richmond, CA). They were discharged at constant resistance mode (2640 Ω) and also under constant current modes (1.8, 3.6 and 7.2 mA, respectively). For the

measurement of the electrochemical performance under bending, the batteries were firmly attached over a cylindrical solid substrate of predetermined curvature.

## 3.3 Choice of Materials and Optimization

### 3.3.1 Nano-carbons

The battery structure, bendable electrodes, separator and photograph of a final cell are shown in Figure 3.1. SEM images of electrodes are shown in Figure 3.2. All formed good cathode composites with desired flexibility. Nanotubes could be uniformly dispersed in the active cathode material, where the functionalized CNTs showed slightly higher dispersibility. In anode the CNTs dispersed well in presence of the zinc particles and bridged the conductive zinc particles. The EDX data is presented in Table 3.1. It showed that other elements such as Fe existed in original CNTs as impurities which were removed during purification. Acid functionalization introduced more oxygen into the CNTs in the form of COOH groups. The purification in dilute acids was not harsh and did not generate noticeable defects or led to oxidation.

Since $MnO_2$ has low conductivity, conductive additives were added into cathode to reduce the internal resistance of the cell. Different carbon forms were tested and the performances of the batteries were compared. The electrode resistance data for different additives are shown in Table 3.2. The application of raw CNTs instead of graphite brought the resistance down from 30.5 to 0.54 KΩ. Figure 3.3 shows the discharge performance of the cells. This decrease in the cathode resistance was attributed to the fact that the CNTs created a more effective conductive network compared to graphite, leading to better performance. These results demonstrated the advantages of CNTs for electrode applications. Moreover, it has been reported that alkaline metal cations interact with the

phenyl group of the CNTs, resulting cation-π interaction (G. Mpourmpakis et al., 2006) and (G. W. Gokel et al., 2000).

**Table 3.1** EDX Results for CNTs

| Element weight % | Raw CNTs | Purified CNTs | Functionalized CNTs |
|---|---|---|---|
| C | 94.55 | 94.94 | 92.02 |
| O | 1.36 | 2.59 | 6.85 |
| Ni | 3.74 | 2.47 | 1.13 |
| Fe | 0.34 | 0 | 0 |

*Source: Z. Wang et al., 2014*

**Table 3.2** Electrode Resistance of Primary Alkaline Battery Cathodes

| Conductive additive | Graphite [kΩ] | Functionalized CNTs [kΩ] | Purified CNTs [kΩ] | Raw CNTs [kΩ] |
|---|---|---|---|---|
| Resistance | 30.5 | 5.4 | 1.9 | 0.54 |

*Source: Z. Wang et al., 2014*

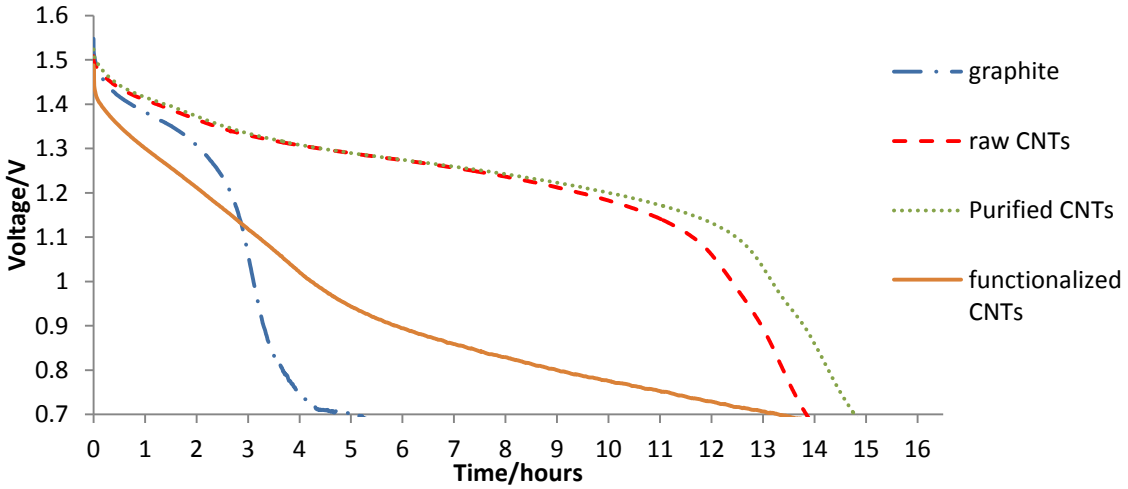


**Figure 3.3** Discharge curves of primary alkaline cells with different carbons (in fixed cells, 2640Ω discharge).
*Source: Z. Wang et al., 2014*

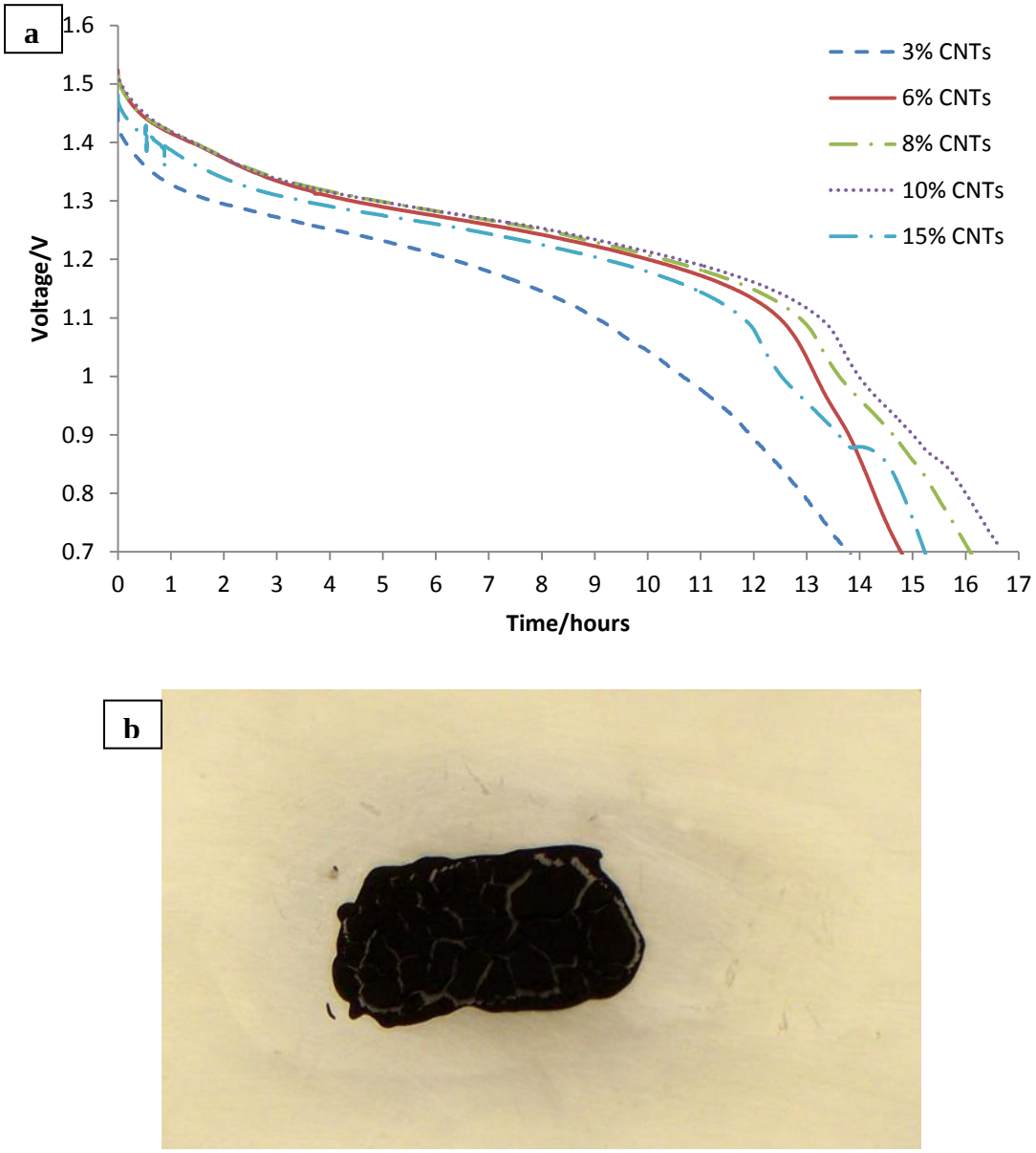


**Figure 3.4** Batteries with different amount of purified CNTs in cathodes: (a) Batteries with different amount of purified CNTs in cathodes (in fixed cells, 2640Ω discharge); (b) cathode cracking at high CNT percent.
*Source: Z. Wang et al., 2014*

Even though the electrode resistance was higher, the purified CNTs showed improvements over the raw CNTs (Figure 3.3). This was due to the removal of the metallic and nontubular carbon impurities. The metals influence the electrochemistry while the graphitic nanoparticles along with amorphous carbon are not as electrically conductive and

do not form uniform composite. The acid treatment generated carboxylic groups on the surface (F. Valentini et al., 2003), making it more hydrophilic. Although there have been reports that the surface oxidation treatment may enhance the electronic conductivity of CNTs composites (Y. Liu, L. Gao, 2005), (Z. Spytalsky et al., 2009) and (Q. Li et al., 2007), in our experiment the functionalized CNTs were not as effective as its non-functionalized analogs. Although the functionalized CNTs showed better dispersion, the oxidative treatment created defects on the CNT surface which disrupted charge transport [Figure 3.2 (b), (c)], thus compromising overall performance. Graphite showed the poorest dispersibility [Figure 3.2 (a)].

**Table 3.3** Specific Performance Data of Different Primary Alkaline Cells

| **Description of the Cell** | **Specific Energy (mWh $g^{-1}$ cathode)** | **Specific Capacity (mAh $g^{-1}$ cathode)** | **Specific Capacity (mAh $g^{-1}$ $MnO_2$)** | **$MnO_2$ utilization (%)** |
|---|---|---|---|---|
| 6% Graphite | 71.3 | 54.3 | 64.7 | 21.0 |
| 6% MWCNTs-raw | 259 | 205 | 244 | 79.2 |
| 6% MWCNTs-COOH | 96.0 | 83.7 | 99.6 | 32.3 |
| 6% MWCNTs-purified | 275 | 218 | 259 | 84.1 |
| 3% MWCNTs-purified | 213 | 178 | 205 | 66.6 |
| 8% MWCNTs-purified | 289 | 230 | 281 | 91.2 |
| 10% MWCNTs-purified | 297 | 236 | 295 | 95.6 |
| 15% MWCNTs-purified | 261 | 211 | 281 | 91.2 |

*Source: Z. Wang et al., 2014*

Increasing the concentration of CNTs resulted in a higher operation voltage and higher discharge capacity. However, for the same electrode weight, as the concentration CNT increased, the amount of active material decreased, which reduced the overall

capacity of the cell (Figure 3.4). At higher CNTs loading, the electrode materials became more fragile which compromised the flexibility. Electrodes with more than 10% CNTs disintegrated easily. The hollow structures of CNTs allowed it to hold the electrolyte and enhance the discharge performance, at the same time the electrodes swelled as they soaked up water, and shrank as they dried out. This led to electrode cracking when there was insufficient binder to hold it together [Figure 3.4 (b)]. That could explain why the performance of electrodes with 15% CNTs was not as good as those at lower concentrations. To avoid this and maintain electrode flexibility, more binder was required and this decreased the conductivity and chemical reactivity. Similar was the situation with the anode.

Zinc was consumed as the battery discharged, and zinc oxide was formed which increased the internal resistance. Therefore, excess zinc was applied to the anode to maintain the electrode conductivity. Gas evolution in alkaline batteries is known to be a problem, excess ZnO has been reported to hinder zinc corrosion, and a decrease in KOH concentration is known to decrease hydrogen generation (V. Ravindran, V. S. Muralidharan, 1995). Anodic corrosion can be inhibited by the addition of certain organic compounds or metals such as Bi, Pb, Al (A. R. Suresh Kannan et al., 1995), (J. Y. Huot, E. Boubour, 1997), and (J. Dobryszyckia, S. Biallozor, 2001). The organic and metal oxides inhibitors are nonconductive and together with polyethylene oxide (PEO) and the zinc oxide generated during the reaction, they increase the anode resistance. In order to lower the resistance, small amount of CNTs were added into the anode (Figure 3.5). In most cases, higher binder concentration led to higher flexibility but lower conductivity and performance. In other cases when there was insufficient binder, the electrode was

susceptible to cracking as shown in Figure 3.4 (b), which invariably led to a decrease in the discharge performance. That was the reason why the discharge performance increased when the PEO ratio increased. Effects of binder concentration are also shown in Figure 3.5, where 6% w/w graphite was used in the cathode. Finally the formulation with 4% PEO and 2% CNTs showed optimum performance and flexibility.

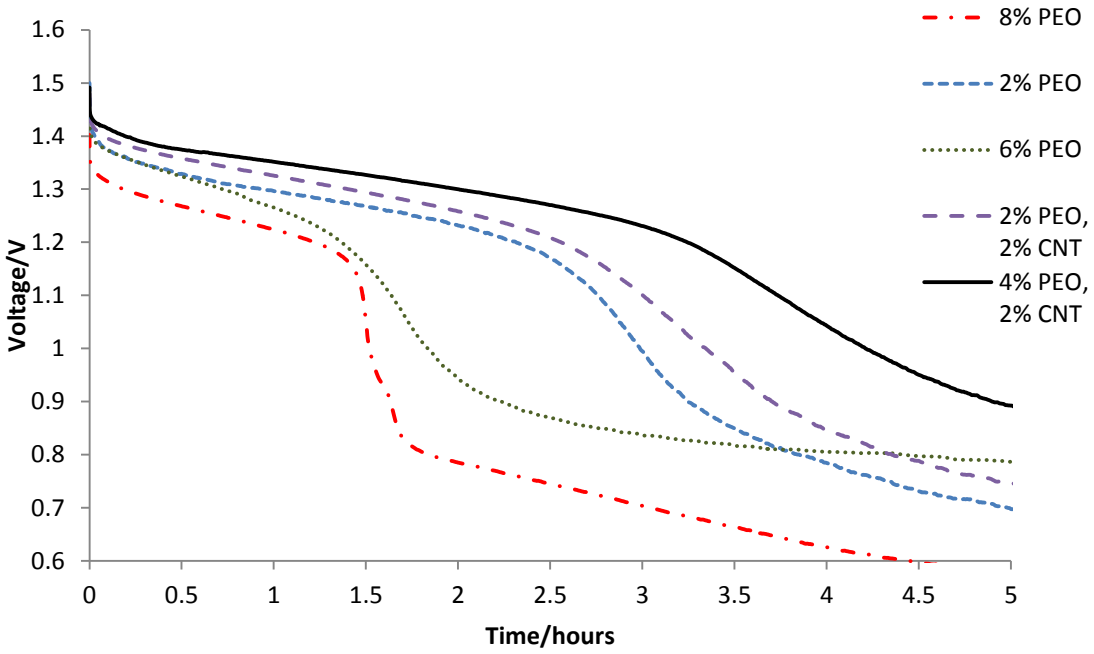


**Figure 3.5** Effects of PEO binder and CNTs in anode (in fixed cells, 2640Ω discharge).
*Source: Z. Wang et al., 2014*

Optimizing the particle size of zinc was important for controlling gas generation. Smaller, micron size particles [Figure 3.2 (d)] with larger surface area facilitated discharge and promoted flexibility. However, zinc nanoparticles enhanced gassing significantly and batteries ceased to work soon.

### 3.3.2 Polymers

The Fourier transform infrared (FTIR) spectra of the copolymer separator are shown in Figure 3.6. The peaks between 1700 and 1750 $cm^{-1}$ were attributed to be the carbonyl C=O bonds, while the peaks between 1300 and 1000 $cm^{-1}$ represent the C-O single bonds. The C=O peaks in PVA spectrum can be attributed to residual acetyl in PVA. Shifts in certain peaks were observed after the esterification reaction. The acid carbonyl peak at 1717.50 $cm^{-1}$ shifted to a higher wavenumber of 1731.96 $cm^{-1}$. The reaction shifted the C–O stretch and led to the appearance of two bands at 1257.70 and 1096.66 $cm^{-1}$. The esterification also weakened the alcohol C-O single bond absorption between 1050 and 1150 $cm^{-1}$.

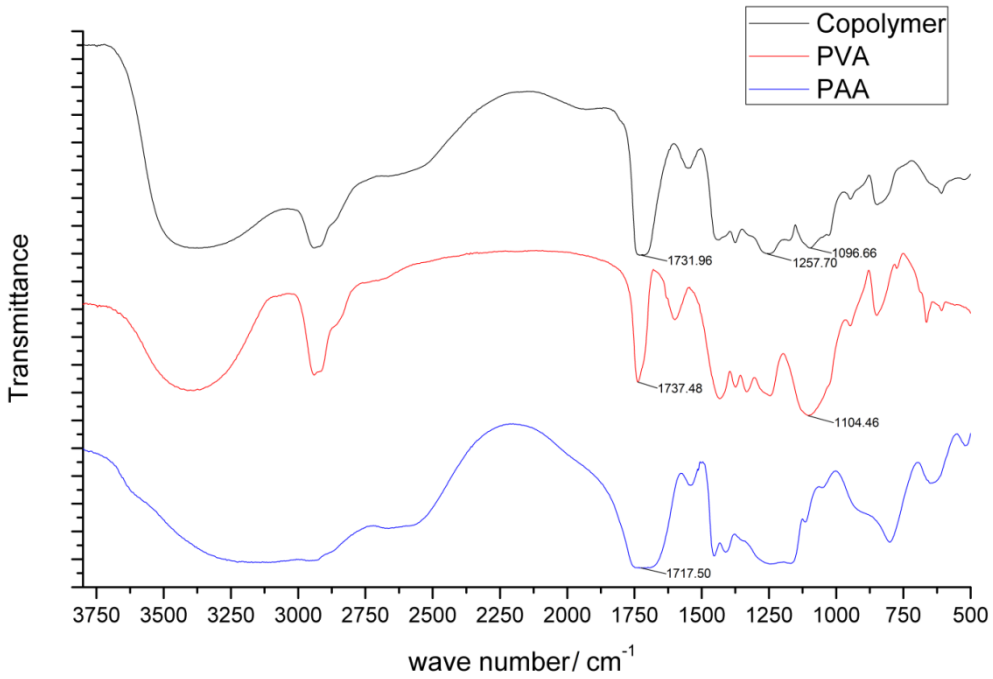


**Figure 3.6** FTIR spectrums for PVA, PAA and the copolymer separator.
*Source: Z. Wang et al., 2014*

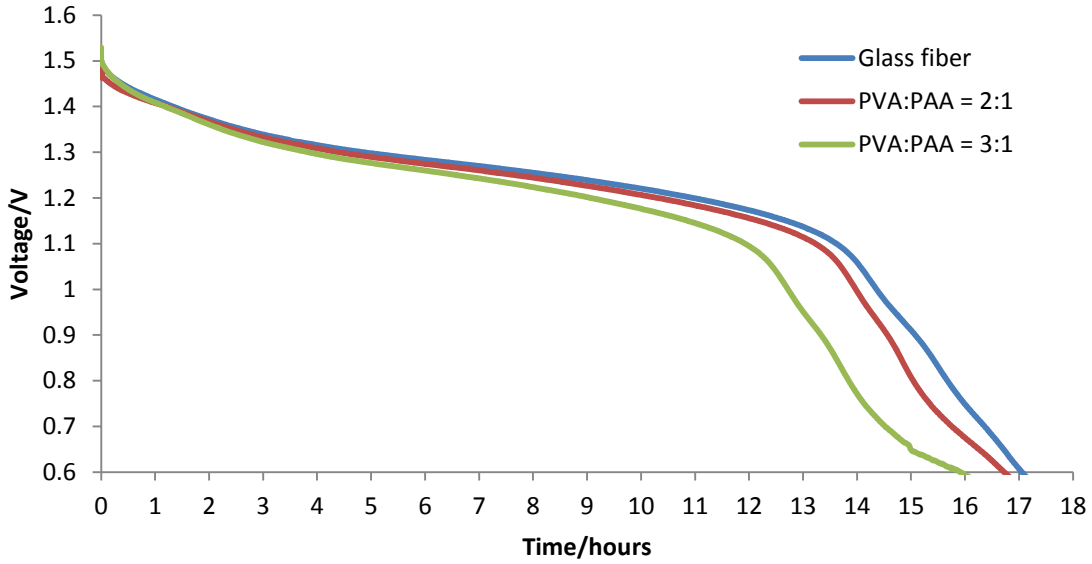


**Figure 3.7** Cells with polymer separator/ glass fiber separator.
*Source: Z. Wang et al., 2014*

The discharge curves in Figure 3.7 show that PVA-PAA copolymer film had similar performance to glass fiber separator. However, the mechanical strength of the PVA-PAA was higher and it had flexibility compared to glass fiber or filter paper separator, and remained stable in the basic environment. Thicker separator held more electrolyte but compromised thickness and flexibility. According to our experimental results, 1 g of the dry PVP-PAA separator could absorb and hold approximately 2.3 g of electrolyte. The SEM image of such a separator is shown in Figure 3.2 (f). The separator also remained stable in the electrolyte. In one experiment, the separator which was soaked in the electrolyte for 1 month showed no sign of decomposition.

### 3.3.3 Flexible Cell Performance

A constant resistance discharge pattern of a flexible battery through a 2640 Ω is shown in Figure 3.8. With an optimized formulation and copolymer separator, a 3 × 4 $cm^2$, 3.3 g

flexible battery lasted as long as 155 hours. The capacity of a flexible battery obtained for optimized anode and cathode with 8% purified CNTs (283 mAh $g^{-1}$) corresponded to the utilization of 92% of the theoretical capacity of $MnO_2$ (308 mAh $g^{-1}$) under a 3.6mA constant current discharge with a cut off voltage 0.9 V (Figure 3.9). This was higher than the zinc carbon battery in the former chapter. Discharge performances at different discharge rates are shown in Figure 3.9.

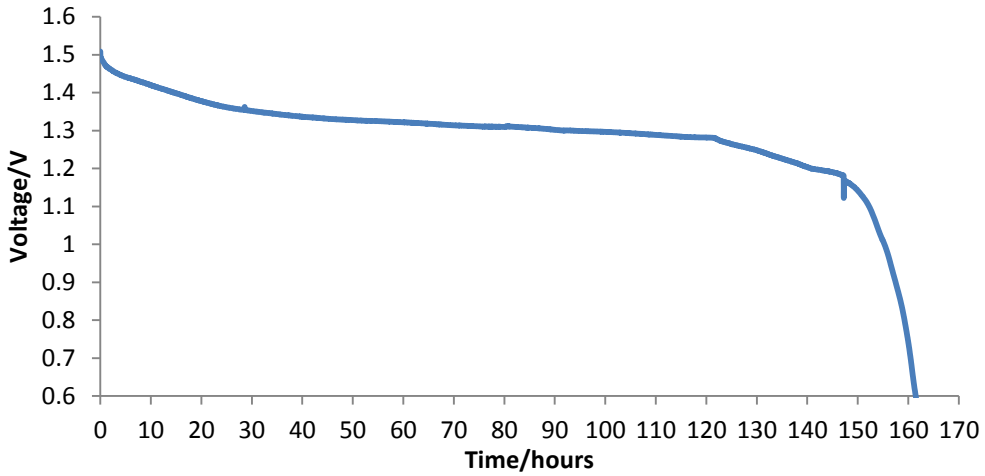


**Figure 3.8** A flexible battery discharged under 2640Ω constant resistance discharge.
*Source: Z. Wang et al., 2014*

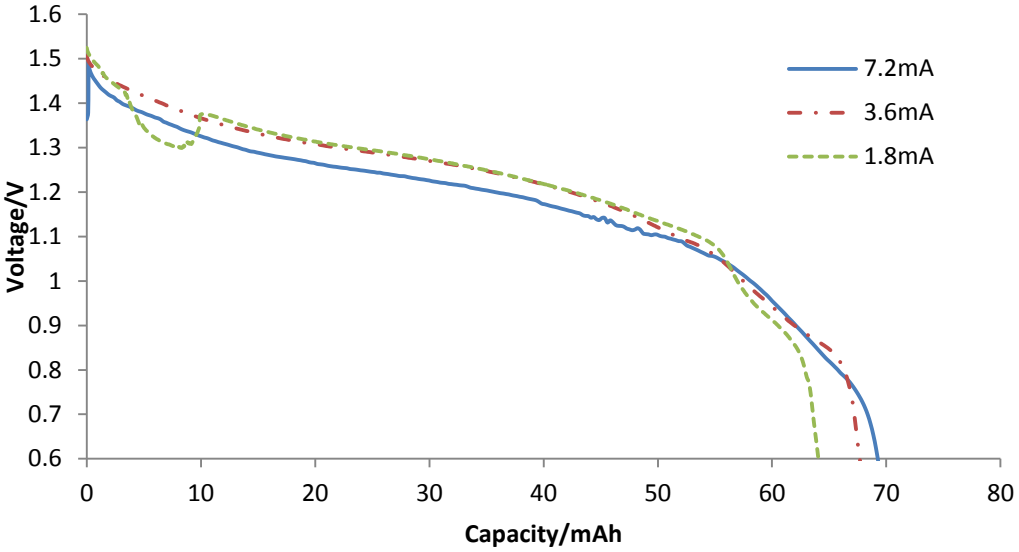


**Figure 3.9** Flexible primary alkaline cell discharge curves under different currents.
*Source: Z. Wang et al., 2014*

Discharge tests under bending conditions (3.6 mA) revealed that the batteries remained functional (Figure 3.10). Two batteries connected in serial can light up LED lights as shown in Figure 3.11. The overall flexibility of the battery depends on the mechanical properties of each component: electrodes, electrolyte, separator and substrate/packaging. The electrodes, substrate and separator showed acceptable flexibility. Bending could induce a compression of the cell stacking enhancing the contact between the particles and between the electrodes and the separator. However, it may also cause cracking in the electrode materials due to the stress. The bending test showed that batteries remained functional, though some voltage fluctuations were observed. PEO, though water soluble, did not dissolve in high concentration salt or in basic solutions, making it an effective binder in flexible battery. In one of our tests, a free-standing PEO film also remained stable in KOH solution. It is the opinion of the authors that the bending performance can be further improved by further optimization of the electrolyte/ separator and by the utilization of more effective sealing system.

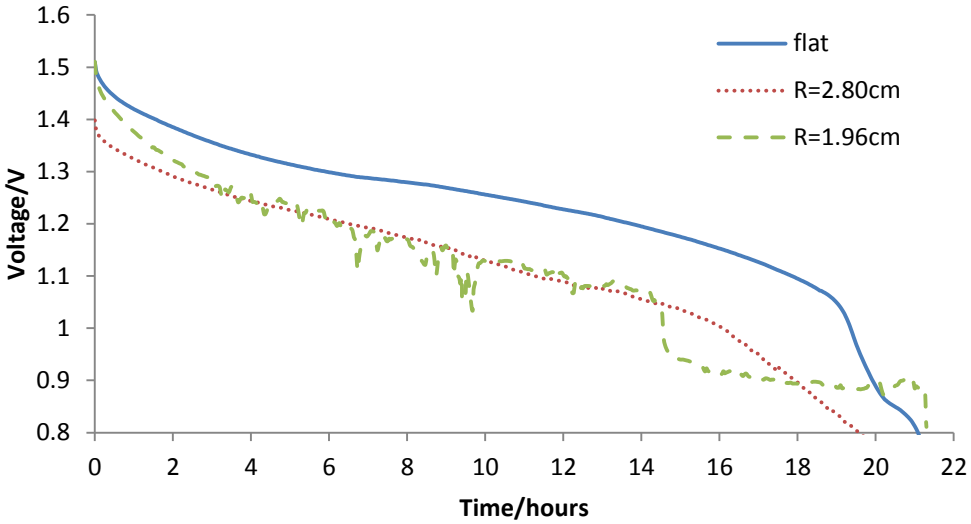


**Figure 3.10** Flexible primary alkaline cells under bending conditions.
*Source: Z. Wang et al., 2014*

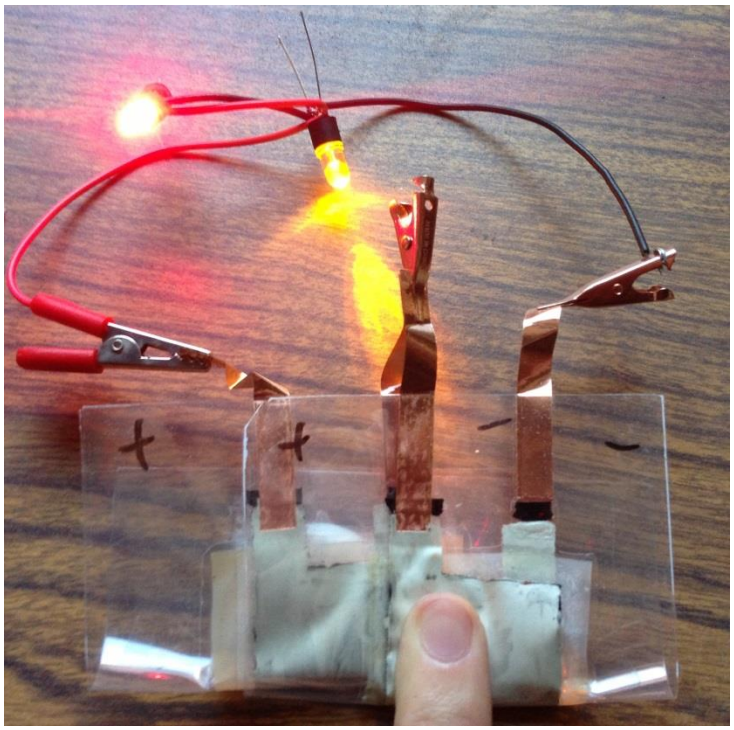

**Figure 3.11** LED demos with flexible primary alkaline batteries.
*Source: Z. Wang et al., 2014*

A new flexible alkaline battery with CNTs in electrode formulation and a novel separator is reported. The CNTs showed some excellent performance and utilization of $MnO_2$ reached as high as 92%. The PVA-PAA copolymer not only was an effective separator but also served as a means of electrolyte storage, ensuring the flexibility of the battery without performance compromise. The formulation of the alkaline battery is such that it could be printed using conventional techniques such as screen, stencil and ink dispensing printing.

# CHAPTER 4

# FLEXIBLE SECONDARY ALKALINE BATTERIES

## 4.1 Background

Secondary alkaline batteries which use $MnO_2$ as active cathode material, Zn anode and alkaline electrolyte are an attractive alternative to lithium ion batteries (F. Beck, P. Rüetschi, 2000), (Y. Shen, K. Kordesch, 2000), (M. Ghaemi et al., 2003). Unlike the latter which have to be charged before the first use, the secondary alkaline batteries can be used out of the package. Similar to zinc-carbon cells, they are suitable for low drain and intermittent devices, and the costs of secondary alkaline batteries are relatively low. Known to work well for less deep discharges and frequent charges, secondary alkaline batteries are considered a good option in many applications including interfacing to solar cells (X.C. Lau et al., 2013), (G. Dennler et al., 2007). Moreover, the secondary alkaline batteries are considered more eco-friendly than their lithium-ion counterparts where lithium is relatively toxic and organic electrolytes are used.

The electrodes of these secondary batteries are similar to their primary counterparts, with small modifications in formulations to acquire rechargeability. Hence, chemical reactions are same as in primary cells except that during the charging process, reactions go in the opposite direction.

## 4.2 Fabrication of Secondary Alkaline Cells

The cathode paste was prepared by mixing EMD, PEO binder, magnesium oxide (Sigma Aldrich, 99.99%) and conductive additives. The conductive additives included synthetic graphite, multiwalled carbon nanotubes (MWCNTs), and carbon black (Sigma Aldrich,

<500 nm). All chemicals were used as received, except that some of the MWCNTs were purified or functionalized prior to the electrode preparation.

The purification and functionalization of CNTs were performed in a Microwave Accelerated Reaction System (Mode: CEM Mars) using experimental procedures same as Chapter 3. After mixing the components in DI water, the paste was sonicated for at least 30 minutes using an ultrasonic homogenizer (Omni Sonic Ruptor 250) and then stirred for 20 hours to form homogenous slurry. The dry cathode contained 2.0% by weight of MgO, 10% PEO, and the rest was EMD and conductive additives. The EMD to conductive additive ratios in the cathode mixture were varied and optimized.

The anode paste was prepared with zinc powder (Sigma Aldrich, ≤10 μm, ≥ 98%), PEO binder, zinc oxide powder (Sigma Aldrich, ≥ 99%), methyl cellulose (Sigma Aldrich, Mn~40,000), Bismuth (III) oxide (Sigma Aldrich, 90-210 nm particle size, ≥ 99.8%) inhibitors, and conductive additives. The powders were mixed in the presence of DI water and then stirred to form a homogeneous anode paste. A typical dry anode contained 1% methyl cellulose, 5% PEO and 2% Bismuth (III) oxide. The amount of zinc, zinc oxide, conductive additives were subject to optimization.

The PVA- PAA (Sigma Aldrich, Mv~450,000) copolymer separator was fabricated using the same method as Chapter 3. The separator was soaked in the electrolyte for 2 hours and cut into right sizes before use. A typical separator after soaking and cutting was 5 cm × 4 cm in size.

Swagelok-type cells using graphite rod current collectors were assembled to optimize the electrode formulation. For anode optimization, the cathode was fixed as 80% EMD, 2% MgO, 8% MWCNTs, and 10% PEO. Typical anode contained 2% $Bi_2O_3$, 5%

PEO and 1% methyl cellulose unless otherwise specified. The amounts of carbons, Zn and ZnO were varied. For cathode optimization, the anode contained 72% Zn, 18% ZnO, 5% PEO, 2% MWCNTs, 1% methyl cellulose, 2% $Bi_2O_3$; cathode contained 2% MgO and 10% PEO while the amount of carbons and EMD were varied. The typical weights of the cathode and anode after drying were 0.03 g and 0.05 g, respectively. The electrolyte was 9 M KOH solution with 6% ZnO.

Flexible electrodes were prepared by casting the electrode slurry onto the silver ink current collectors. The current collectors were prepared by manually applying silver ink to the adhesive side of polyethylene terephthalate (PET) film coated with ethylene vinyl acetate copolymer (EVA) resin (CRC52005, 3 mil, Fellowes) to form a layer with silver loading of 3.6 mg $cm^{-2}$. The typical electrode area was 4 cm × 3 cm. Copper tapes (EMI Copper Foil Shielding Tape 1181, 6.35mm, 3M™) were stuck to the current collector to serve as electrode tabs. After applying the slurry onto the current collector, the electrodes were allowed to dry at ~50°C for 30 minutes. The last 5 minutes of drying was processed under vacuum (9.893 kPa). The drying was complete with no residual water. The typical weights of the cathode and anode after drying were 0.06 g and 0.125 g, respectively. The battery was thermally sealed. In all the cells tested, zinc was in stoichiometric excess and there was enough to maintain the required anode conductivity, so in the electrochemical process $MnO_2$ was considered to be the limiting reagent.

Scanning electron microscope (SEM) images were collected on a LEO 1530 VP Scanning Electron Microscope. The electrochemical performances of the cells were measured by discharging and charging under constant current modes using a MTI Battery Analyzer (Richmond, CA). The fixed Swagelok-type cells were discharges at 1.48 mA to

0.9 V and overcharged at 2.96 mA to 2 V; while the flexible ones were discharged and charged at 4 and 8 mA, respectively. The flexible batteries were also firmly attached over solid substrates of different shapes like and tested to examine electrochemical performance under bending conditions.

### 4.3 Further Optimization

The flexible separator which was electrically nonconductive but had high ionic conductivity was placed between the electrodes and the whole assembly needs to demonstrate flexibility. Again the PVA-PAA copolymer film served as a separator as well as a medium for electrolyte storage, and it maintained its stability and flexibility. It was found that this film could also be a promising candidate for the secondary cells.

Figure 4.1 (a-c) shows scanning electron microscopy (SEM) images of cathodes formulated with different nano-carbons. Table 4.1 shows the energy-dispersive X-ray spectroscopy (EDX) data of different carbon nanotubes used to make cathodes. Acid functionalization introduced more oxygen into the CNTs in the form of COOH groups. The purification in dilute acids was only to remove impurities including metal oxides. These conductive additives were added into cathode to reduce the internal resistance.

The constant current discharge-charge curve of an alkaline cell is shown in Figure 4.2. This typical cell contained 6% MWCNTs and 2% carbon black as conductive additives in the cathode, the anode contained zinc, zinc oxide as well as 2% MWCNTs, and the copolymer separator was placed between them. The red curve shows the charge-discharge voltage patterns as a function of time, while the blue curve shows the delivered capacity of each cycle in mAh. A cell was discharged to 0.9 V and recharged to 2 V to form a single

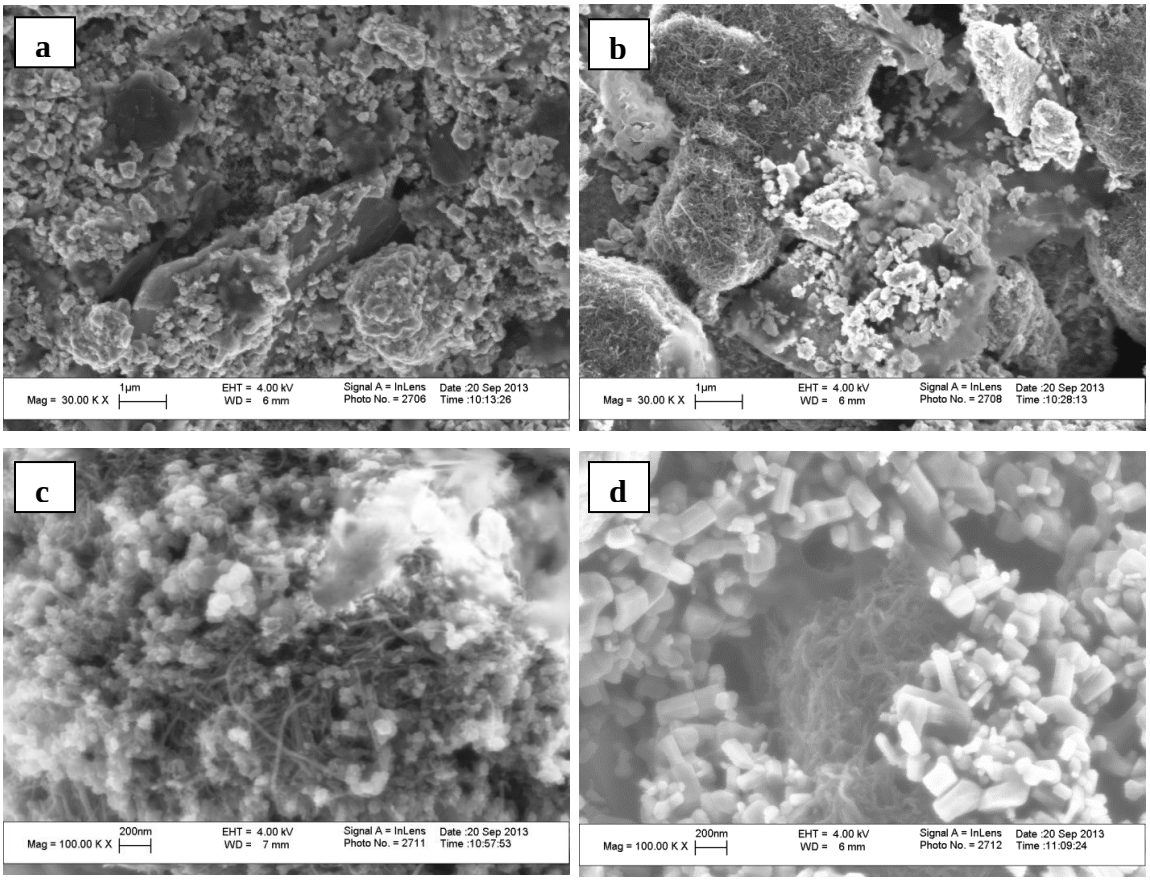


**Figure 4.1** SEM images of secondary alkaline battery electrodes: (a) cathode with graphite and carbon black; (b) cathode with MWCNTs; (c) cathode with carbon black and MWCNTs; (d) MWCNTs in anode.
*Source: Z. Wang, S. Mitra, 2014*

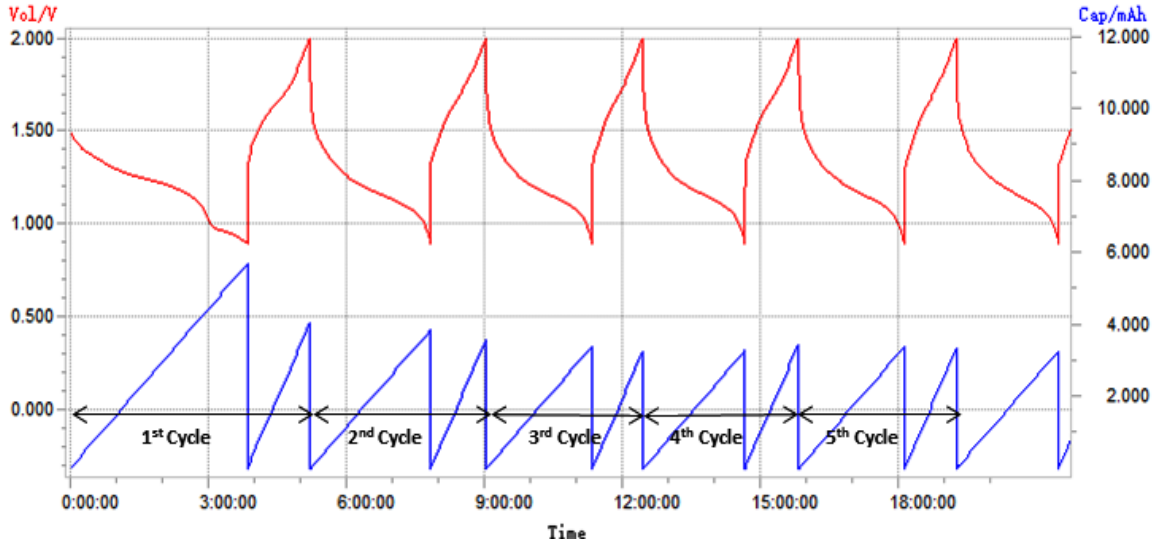


**Figure 4.2** Discharge and charge curves of a secondary alkaline cell.
*Source: Z. Wang, S. Mitra, 2014*

**Table 4.1** EDX Data of Different MWCNTs

| CNTs | C weight % | O weight % | Fe weight % | Ni weight % |
|---|---|---|---|---|
| CNT-raw | 96.57 | 1.34 | 0.19 | 1.90 |
| CNT-purified | 97.66 | 0.82 | - | 1.52 |
| CNT-COOH | 86.81 | 13.19 | - | - |

*Source: Z. Wang, S. Mitra, 2014*

**Table 4.2** Capacity of Secondary Alkaline Cells with Different Carbons in Cathode

| Cells | Theoretical Capacity (mAh) | Delivered Capacity 1st cycle (mAh) | Delivered Capacity 25th cycle (mAh) | Specific Capacity of $MnO_2$ (mAh $g^{-1}$) 25th cycle |
|---|---|---|---|---|
| 2% carbon black + 6% CNT- purified | 6.8 | 5.85 | 2.478 | 112.2 |
| 8% CNT- purified | 6.8 | 5.111 | 1.891 | 85.7 |
| 8% CNT- raw | 6.8 | 4.235 | 1.36 | 61.6 |
| 2% carbon black + 6% graphite | 6.8 | 4.279 | 1.708 | 77.4 |
| 8% carbon black | 6.8 | 4.721 | 1.937 | 87.7 |
| 8% CNT- COOH | 6.8 | 2.055 | 0.128 | 5.8 |

*Source: Z. Wang, S. Mitra, 2014*

cycle. The discharge pattern of the single cycle was similar to what had been shown in Chapter 3.

Performances of different cells with different carbon forms are shown in Figure 4.3, with theoretical capacity in Table 4.2. It shows delivered cell capacity during each discharge as a function of cycle number. Graphite which has been extensively used together with carbon black in rechargeable alkaline batteries showed lower performance than the MWCNTs. The replacement of graphite by MWCNTs improved the cell

performance. The purification of CNTs removed impurities which might have hindered the electrochemical reactions and therefore enhanced cell performance even further.

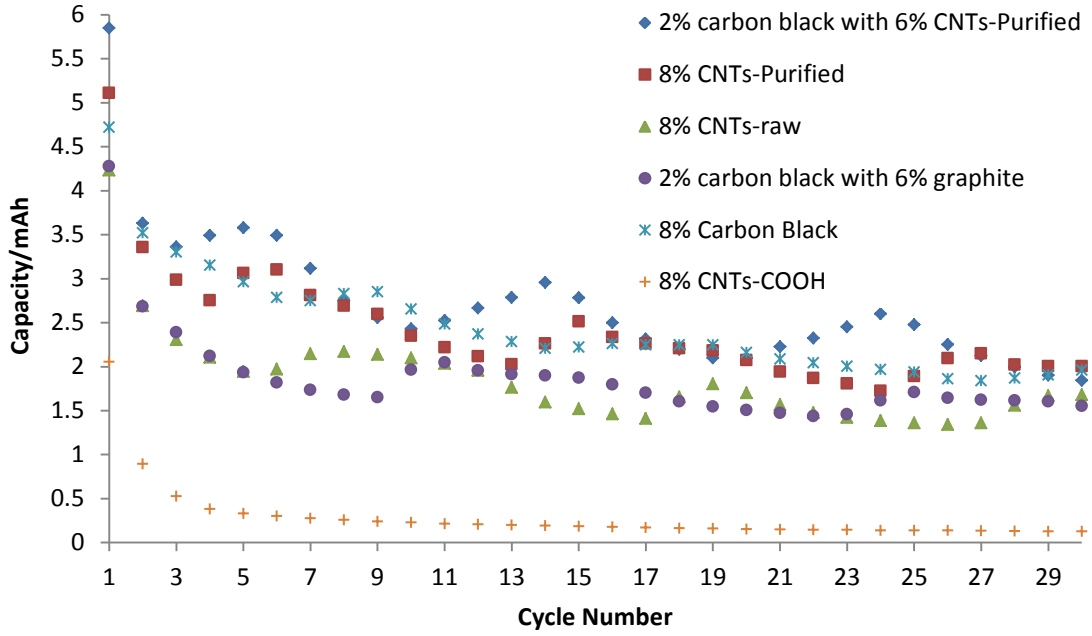


**Figure 4.3** Capacity as a function of cycle numbers for cells with different carbons.
*Source: Z. Wang, S. Mitra, 2014*

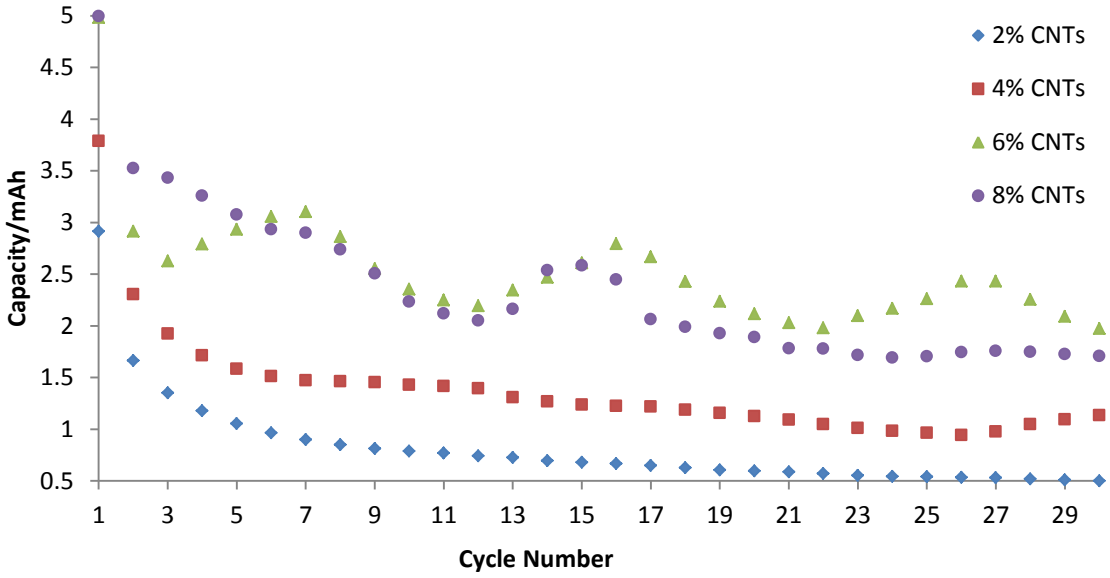


**Figure 4.4** Cycling of cells with cathodes containing purified CNTs and 2% carbon black.
*Source: Z. Wang, S. Mitra, 2014*

**Table 4.3** Capacity of Secondary Alkaline Cells with Purified CNTs in Cathode

| Cells | Theoretical Capacity (mAh) | Delivered Capacity 1st cycle (mAh) | Delivered Capacity 25th cycle (mAh) | Specific Capacity of $MnO_2$ (mAh $g^{-1}$) 25th cycle |
|---|---|---|---|---|
| 2% CNTs | 7.31 | 2.915 | 0.538 | 22.7 |
| 4% CNTs | 7.14 | 3.787 | 0.962 | 41.5 |
| 6% CNTs | 6.8 | 4.982 | 2.26 | 102.4 |
| 8% CNTs | 6.63 | 4.994 | 1.7 | 79 |

*Source: Z. Wang, S. Mitra, 2014*

**Table 4.4** Capacity of Secondary Alkaline Cells with 2% CNTs in Anode

| Cells | Theoretical Capacity (mAh) | Delivered Capacity 1st cycle (mAh) | Delivered Capacity 25th cycle (mAh) | Specific Capacity of $MnO_2$ (mAh $g^{-1}$) 25th cycle |
|---|---|---|---|---|
| 2% CNTs-raw | 6.8 | 4.247 | 1.735 | 78.6 |
| 2% CNTs-COOH | 6.8 | 4.715 | 1.524 | 69 |
| 2% CNTs-purified | 6.8 | 3.273 | 1.802 | 81.5 |

*Source: Z. Wang, S. Mitra, 2014*

The functionalized CNTs showed lower performance due to the defects that lead to lower conductivity. Even in the first discharge, cells with functionalized CNTs showed lower capacity just like the primary cells described in Chapter 2 and Chapter 3. This was different from lithium-ion batteries where higher levels of defects were known to enhance capacity (B. J. Landi et al., 2009) and (S. L. Candelaria et al., 2012). Rechargeability was also compromised by the surface defects and higher resistance due to functionalization. The poor conductivity made electron transfer from $Mn_2O_3$ particles more difficult during the charging cycle. The interaction between the alkaline electrolyte and the carboxylic groups on the CNTs may have also contributed to the degradation in performance. The electrolyte may have been partially neutralized causing a drop in surface concentration of

$OH^-$, which reacted with $Mn_2O_3$ during the charging. The negative charge of $COO^-$ groups might also repel the $OH^-$.

It has been mentioned in Chapter 3 that the flexible battery electrodes tend to become fragile at high concentration of conductive additives thus decreasing the discharge performance. As a conductive additive carbon black showed good performance, yet the electrodes were found to be more fragile than their MWCNT counterparts. Experiment results indicated that cathode with 6% purified MWCNTs and 2% carbon black showed optimum performance and flexibility (Figure 4.4 and Table 4.3). CNTs and carbon black were more effective as conductive additives than graphite due to their better dispersibility. CNTs were dispersed together with carbon black in the cathode. The latter filled the small gaps and connected to conductive networks formed by CNTs. The unique shape of CNTs maintained the integrity of the electrodes during bending and imparted good mechanical properties. In another set of tests, when carbon black alone was used as the conductive additive, the electrode was more fragile and less effective under bending conditions. The CNTs and the carbon black also appeared to disperse well with $MnO_2$ and the long CNTs helped bridge the carbon black particles and formed better conductive networks. Electrode with 8% purified MWCNTs and 2% carbon black showed similar performance but capacity faded faster while the electrode flexibility was lower. Compared to primary cells in Chapter 3, the active material utilization was lower in the rechargeable batteries even in the first discharge, which could be partially attributed to the much higher amounts of non-conductive agents added to the electrode. For a cell with optimized formulation (consider electrode performance and flexibility), the first discharge showed approximately 79% utilization (243 mAh $g^{-1}$) of limiting active material manganese dioxide. This dropped

to 38% (117 mAh $g^{-1}$) after the first 10 cycles, and after 30 cycles the manganese dioxide specific capacity dropped to approximately 105 mAh $g^{-1}$, which was 34% of the theoretical value of 308 mAh $g^{-1}$ $MnO_2$. These values were similar to those reported for conventional (nonflexible) secondary alkaline cell electrodes (200-225 mAh $g^{-1}$ during the first discharge; 75-125 mAh $g^{-1}$ after 25 cycles (A. Stani et al., 2006); and even lower elsewhere (M. Ghaemi et al., 2003).

Flexible Anode: The MWCNTs dispersed well with the micron-sized zinc and bridged the conductive particles [Figure 4.1 (d)]. Zinc was oxidized to zinc oxide during discharge. Other composites such as PEO, methyl cellulose and $Bi_2O_3$ were non-conductive. In order to maintain the anode conductivity, MWCNTs were added into the anode. Three different CNTs were tested (Figure 4.5 and Table 4.4). Unlike the cathode, the purification of CNTs appeared to provide little improvement. However, the residual metal catalysts in the CNT preparation might have caused secondary reactions or self-discharge and therefore the purification of CNTs was still important. CNT-COOH showed better performance during the first 10 cycles; however, the capacity faded faster. It is concluded that during the beginning cycles with sufficient zinc and electrolyte, the lower conductivity of CNT-COOH was compromised by the higher conductivity of zinc. During the following cycles when zinc was consumed or coated with zinc oxide, the electrode conductivity decreased and CNT-COOH was not as good a conductive additive as the other CNTs.

An increase in the amount of CNTs added to the anode compromised electrode flexibility just like it did in the cathode. A concentration of 2% MWCNTs in the anode was a balance between optimum performance and flexibility (Figure 4.6 and Table 4.5).

Without CNTs, the cell capacity faded rather quickly. The CNTs also led to optimum viscosity which allowed easier casting, helped prevent the formation of an impervious Zn/ZnO layer, and kept channels open for electrolyte diffusion.

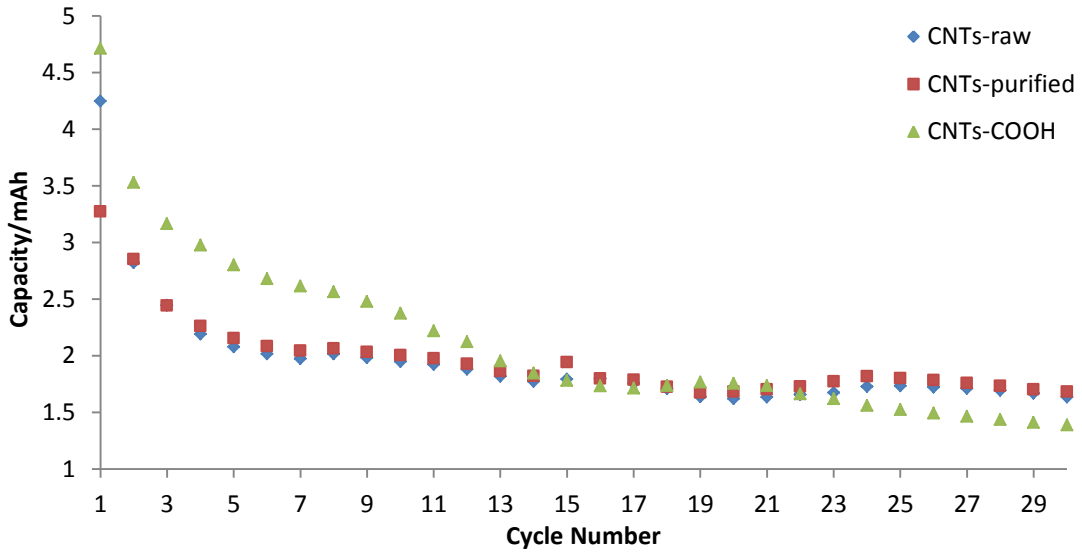


**Figure 4.5** Cycling of cells with 2% CNTs in anode.
*Source: Z. Wang, S. Mitra, 2014*

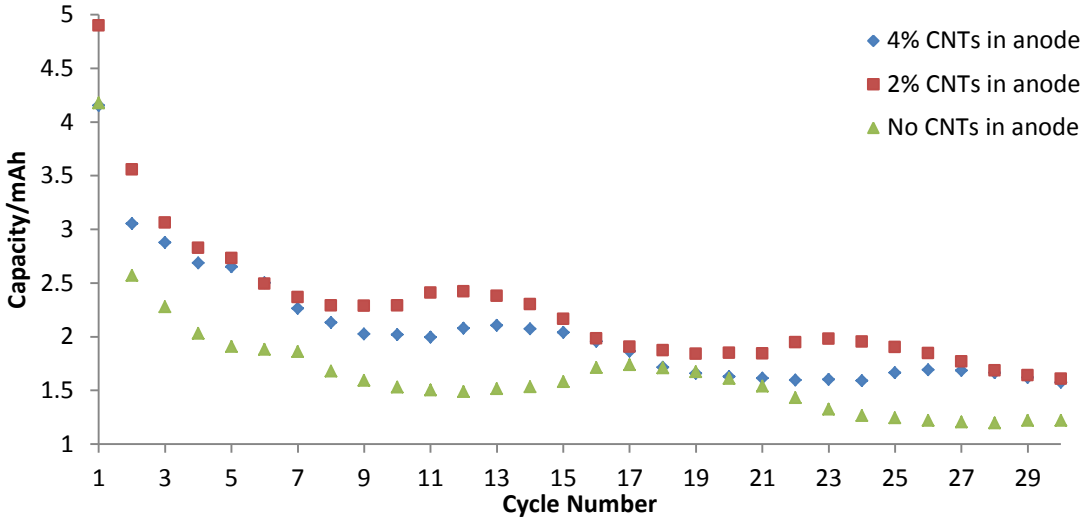


**Figure 4.6** Secondary alkaline cells with purified CNTs in anode.
*Source: Z. Wang, S. Mitra, 2014*

Different Zn to ZnO ratios were also used to optimize the anode formulation. The performance of cells with different Zn/ZnO ratio is shown in Figure 4.7 and Table 4.6. ZnO was critical to inhibiting gassing. While it could be reduced back to zinc during charging; it

could also reduce the available amount of electrolyte. ZnO is known to react with $OH^-$ to form zincates which is a common occurrence in all alkaline cells (M. Ghaemi et al., 2003), (R. Shivkumar et al., 1995). Cells with a Zn to ZnO ratio of 5:1 showed the best rechargeability, which was followed closely by a 4:1 ratio. Cells with higher amount of ZnO showed lower performance due to the low conductivity of ZnO while those with very low ZnO concentration showed poor rechargeability. It is evident that the relatively higher concentration of ZnO in the anode was an important feature of the secondary alkaline cell and was critical for rechargeability.

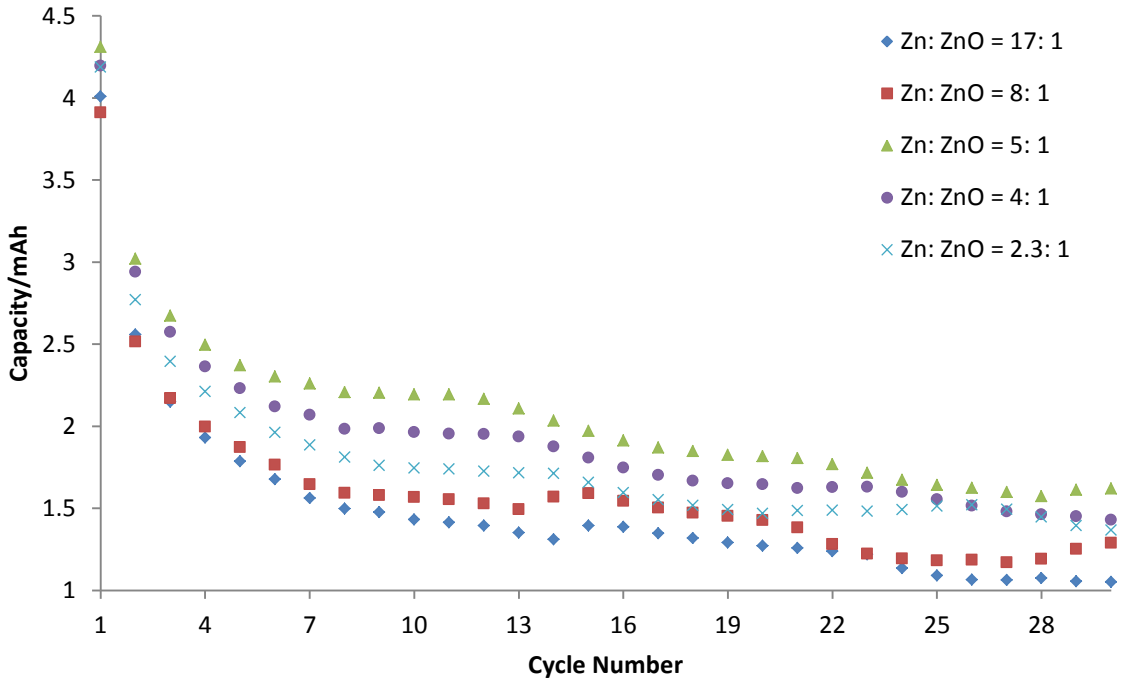


**Figure 4.7** Secondary alkaline cells with different Zn to ZnO ratio in anode (all contained 2% purified CNTs).
*Source: Z. Wang, S. Mitra, 2014*

The capacity is known to fade with discharge-charge cycles in conventional secondary alkaline cells. There are different reports on the mechanisms behind the decrease in capacity with increased cycling. It has been known that soluble zincates enter

into $MnO_2$ lattice and alter the shape of the anode (Y. Shen, K. Kordesch, 2000) (M. Ghaemi et al., 2003). Hence, MgO was added to the cathode to block the incorporation of zincate ions into the $MnO_2$ region (M. Minakshi et al., 2011), while methyl cellulose was added into anode as gelling agent to prevent the alteration of anode morphology (Y. Shen, K. Kordesch, 2000). These were particularly important for reducing capacity fades and ensuring better rechargeability. The degradation of anode materials with cycling is an important issue for all rechargeable batteries. Figure 4.8 (a) shows anode materials after 30 cycles.

Parts of the anode formed hard shell with darker color which is in line with what has been reported elsewhere (Y. Shen, K. Kordesch, 2000). The SEM images of the light and dark parts of the anode are shown in Figure 4.8. The hardened dark parts appeared to be less porous. It is believed that the dark layer is composed of Zn deposits which were formed by the reduction of precipitated ZnO, and such layers are less permeable to electrolytes and hinder further electrochemical reactions (C. Cachet, R. Wiart, et al., 1987, 1988 and 1989). The reduction of this shell is possible with the addition of gelling agents such as methyl cellulose (Y. Shen, K. Kordesch, 2000). As shown in Figure 4.9 and Table 4.7, the cell performance improved with the addition of optimum amount of methyl cellulose. However, addition of very high concentrations of gelling agent made the anode fragile and compromised flexibility. The performance after optimization was in line with what has been reported for conventional batteries by Y. Shen and K. Kordesch.

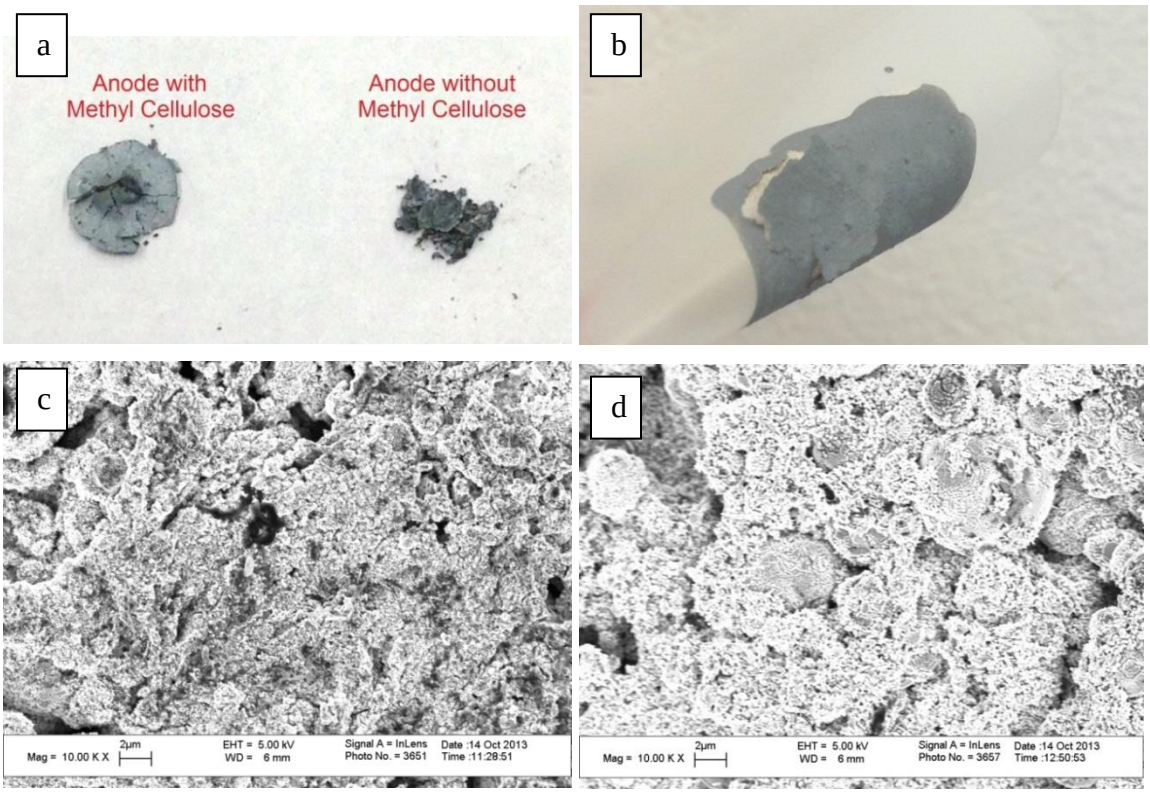


**Figure 4.8** Images of secondary alkaline cell anodes (a) Anode material after 30 cycles; (b) anode material with higher amount of gelling agent; (c) SEM image of lighter part of anode; (d) SEM image of darker part of anode.
*Source: Z. Wang, S. Mitra, 2014*

The separator was an important component of the flexible battery. Cells with traditional glass fiber separator failed but this problem was overcome by using copolymer separator that has been described in Chapter 3 and is not discussed for brevity.

The flexible cells had an open circuit voltage of 1.5 V. Two cells were connected in series to power LED lights as shown in Figure 4.10. The performance of the flexible cell under bending conditions is shown in Figure 4.11. Cells were bent in different ways: they were bent in 90 degrees, folded in half (180 degrees), and rolled into cylinders with a relatively narrow radius of 2 cm. The copolymer separator was effective in the secondary alkaline cell. The flexible cells remained functional under bending and folding conditions; however, the performance were compromised (theoretical capacity was 13.5 mAh). During

bending, parts of the electrodes and separator stacked together and enhanced contact in some sections while other parts separated to lose contact. This caused fluctuation/ drop in cell performance. Another reason was that the packaging techniques allowed relatively lower amount of electrolyte to be incorporated in the cells. Performance could be further improved by improving the internal contacts and electrolyte storage with more advanced packaging methods. The cell performance could also be improved by using $MnO_2$ nanoparticles.

**Table 4.5** Capacity of Secondary Alkaline Cells with Purified CNTs in Anode

| Cells | Theoretical Capacity (mAh) | Delivered Capacity 1st cycle (mAh) | Delivered Capacity 25th cycle (mAh) | Specific Capacity of $MnO_2$ (mAh $g^{-1}$) 25th cycle |
|---|---|---|---|---|
| 0% CNTs | 6.8 | 4.177 | 1.243 | 56.3 |
| 2% CNTs | 6.8 | 4.897 | 1.901 | 86.4 |
| 4% CNTs | 6.8 | 4.151 | 1.662 | 75.3 |

*Source: Z. Wang, S. Mitra, 2014*

**Table 4.6** Capacity of Secondary Alkaline Cells with Different ZnO Contents

| Zn:ZnO ratio of cells | Theoretical Capacity (mAh) | Delivered Capacity 1st cycle (mAh) | Delivered Capacity 25th cycle (mAh) | Specific Capacity of $MnO_2$ (mAh $g^{-1}$) 25th cycle |
|---|---|---|---|---|
| 17:1 | 6.8 | 4.01 | 1.09 | 49.37 |
| 8:1 | 6.8 | 3.912 | 1.182 | 53.54 |
| 5:1 | 6.8 | 4.31 | 1.642 | 74.37 |
| 4:1 | 6.8 | 4.195 | 1.555 | 70.43 |
| 2.3:1 | 6.8 | 4.188 | 1.514 | 68.58 |

*Source: Z. Wang, S. Mitra, 2014*

**Table 4.7** Capacity of Secondary Alkaline Cells with Methyl Cellulose in Anode

| Cells | Theoretical Capacity (mAh) | Delivered Capacity 1st cycle (mAh) | Delivered Capacity 25th cycle (mAh) | Specific Capacity of $MnO_2$ (mAh $g^{-1}$) 25th cycle |
|---|---|---|---|---|
| 0% methyl cellulose | 6.8 | 4.296 | fail | fail |
| 1% methyl cellulose | 6.8 | 5.848 | 2.154 | 97.6 |
| 2% methyl cellulose | 6.8 | 5.155 | 1.975 | 89.5 |
| 2% methyl cellulose with glass fiber separator | 6.8 | 5.474 | 0.723 | 32.7 |

*Source: Z. Wang, S. Mitra, 2014*

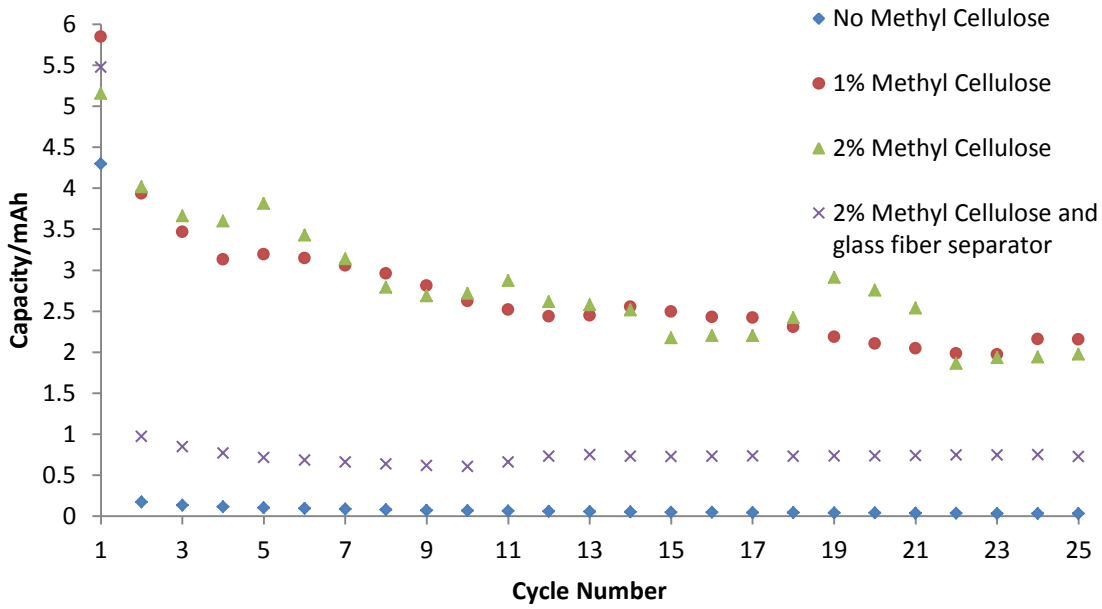


**Figure 4.9** Secondary alkaline cells with methyl cellulose in anode.
*Source: Z. Wang, S. Mitra, 2014*

## 4.4 Conclusions

In summary, flexible secondary alkaline batteries were fabricated successfully. Once optimized, they showed enhancement in both electrode performance and flexibility. Purified multiwalled carbon nanotubes were found to be effective conductive cathode additives in combination with carbon black. The addition of small amounts of carbon

nanotubes also helped anode performance by reducing electrode resistance when the concentration of ZnO was relatively high. The addition of methyl cellulose to the electrodes enhanced rechargeability by providing pathways for electrolyte mobility.

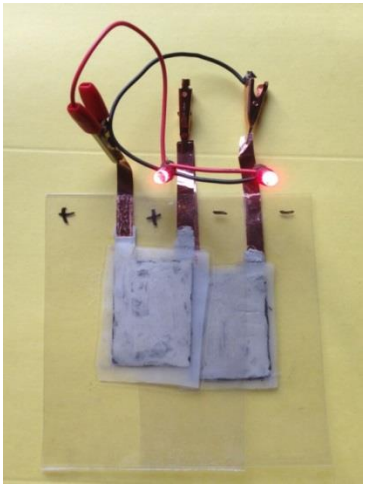


**Figure 4.10** Flexible secondary alkaline batteries powering up LED lights.
Source: Z. Wang, S. Mitra, 2014

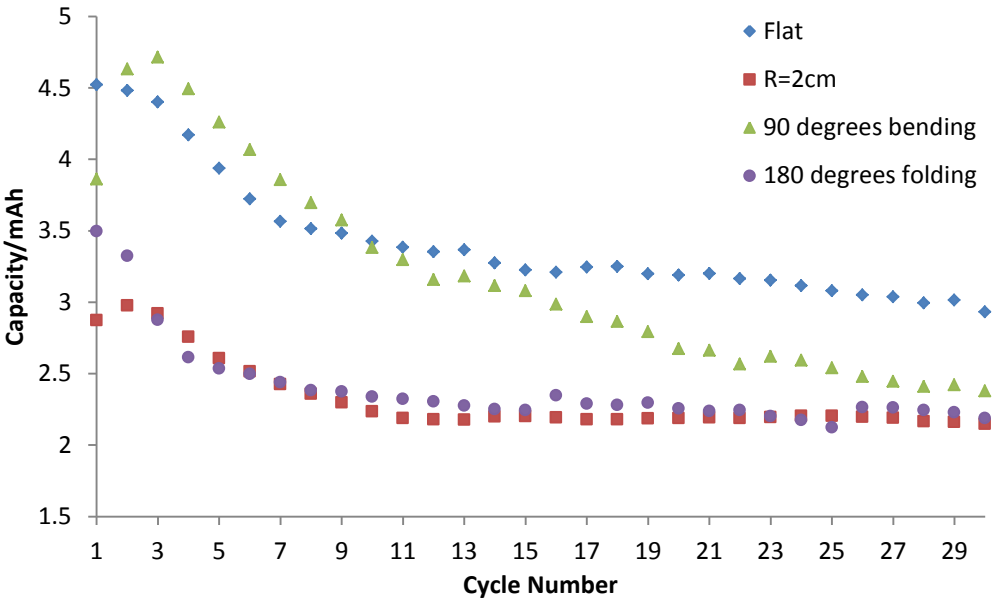


**Figure 4.11** Flexible secondary alkaline cell bending tests.
*Source: Z. Wang, S. Mitra, 2014*

# CHAPTER 5

# CARBON NANOTUBES FOR OTHER POWER SOURCES: SUPERCAPACITORS

## 5.1 Background

Supercapacitors based on double-layer or pseudocapacitance can provide high power densities and discharge currents, and are often used in conjunction with or to replace batteries in many applications (P. Simon, Y. Gogotsi, 2008) and (P. Simon, J. R. Miller, 2008). In the double-layer structure, the energy storage is based on the migration of ions to the electrode surface with no electron transfer between phases. On the other hand, in pseudocapacitance the charge transfer is based on Faradaic reactions at the electrode (V. V. N. Obreja, 2008), (B. E. Conway et al., 1997) and (Y. Zhang et al., 2009). Metal oxides such as $MnO_2$, $Fe_3O_4$ and $RuO_2$ have shown high theoretical capacities and asymmetric supercapacitors using these materials with carbon as the other electrodes have been reported (L. Bao et al., 2011), (J. Zang, X. Li, 2011), (L.Y. Chen et al., 2013) and (J. Jiang et al., 2012). The pseudocapacitance in metal oxide electrodes is based on reversible absorption of atomic species into the crystal structure during redox reactions (B. E. Conway et al., 1997) and (G. Wang et al, 2012).

Since some metal oxides have poor electrical conductivity, different nano-carbons including CNTs and graphene have been used as conductive additives, and the carbon has served as the matrix/scaffolds for the metal oxides (S. L. Candelaria et al., 2012), (K. Gao et al., 2013), ( L. T. Le et al., 2011), (L. Bao, X. Li, 2012) and (M. Zhi et al., 2013). In these cases the metal oxides were coated or incorporated on the surface of nano-carbons to form carbon-metal oxide composites. In other cases the carbons and in particular the CNTs have been used as electrode materials by themselves where they mainly worked through

double-layer capacitance without phase transformation in electrode materials (E. Frackowiak et al., 1999, 2001).

Lithium intercalation into metal oxide electrodes can occur in aqueous as well as organic electrolytes (M. Manickam et al., 2004) and (Y. Wang, J. Yi, Y. Xia, 2012). A carbon/$LiMn_2O_4$ hybrid aqueous electrochemical supercapacitor has been reported. It has potential advantages of high energy density, extended cycle life and fast charge capability (Y. Wang, Y. Xia, 2005). Unlike lithium-ion batteries, here the carbon negative electrode stores charge through a reversible non-faradaic reaction of cations without lithium intercalation or reduction. Surface area, defects and particle size of the carbon have strong effects on the performance of such hybrid supercapacitors. Efforts have gone into improving the performance of CNTs via functionalization to add functional groups and generating defects via conventional chemical techniques such as acid treatment, refluxing and sonication (C. G. Salzmann et al., 2007), (F. Hauke, A. Hirsch, 2010), (A. Stein et al., 2009) and (W. Huang et al., 2002). Many of these reactions are energy and time-consuming. Microwave treatment of CNTs is known to cause in-situ super heating leading to fast reactions with high degree of functionalization (Y. Wang et al., 2005), (Y. Chen, S. Mitra, 2008). Such treatment of CNTs not only generates defects but also introduce oxidative functional groups which may provide pseudocapacitance (E. Frackowiak, 2000). The objective of this research was to study the microwave induced defect generation and oxidative functionalization of CNTs for specific application in supercapacitors.

## 5.2 Carbon Nanotube Supercapacitor Fabrication and Characterization

### 5.2.1 Electrode Preparation and Cell Fabrication

In asymmetric supercapacitors, the $LiMn_2O_4$ cathode paste was prepared by mixing 0.85 g $LiMn_2O_4$ (Sigma Aldrich, 92%, AB Grade), 0.05 g polyethylene oxide (PEO, Sigma Aldrich, Mv~400,000) and 0.1 g conductive additive carbon black (Sigma Aldrich, 500 nm) in 2.4 g poly(3,4-ethylenedioxythiophene)-poly(styrenesulfonate) solution (PEDOT:PSS, Aldrich, 1.3%). Anode paste was prepared by mixing 0.17 g multiwalled CNTs, 0.02 g PEO and 0.01 g carbon black in 0.6 g PEDOT:PSS solution. This anode formulation was also used for both electrodes in the symmetric supercapacitors. Typical electrode weight after drying (60 °C, 9.893 kPa) was 30 mg for asymmetric supercapacitors and 2 mg for symmetric supercapacitors. Glass microfiber filters (Grade GF/A: 1.6 μm, Whatman) were used as separator, with stainless steel rods (12.5 mm diameter) as current collectors and 5 M $LiNO_3$ as electrolyte. Cells were charged/ discharged using a MTI multi-channel Battery Analyzer (Richmond, CA). Electrodes for cyclic voltammetry (CV) were composed of 15% polyvinylidene fluoride (PVDF, Scientific Polymer Products, Inc.) binder, 10% carbon black and 75% CNTs. The total weight for each CV electrode was 3 mg. All electrolyte salts were purchased from Sigma Aldrich.

### 5.2.2 CNT Treatment

Multiwalled CNTs (purity 95%, diameter 20-30 nm, length 10-30 μm, Cheap Tubes Inc. Brattleboro, VT, USA) were used as received, purified or functionalized prior to analysis or electrode preparation. The purification of CNTs was carried out in the microwave

accelerated reaction system by dispersing pre-weighed CNTs into 1 M $HNO_3$; typically 50 ml of acid for 0.3g of CNTs. The reaction vessels were subject to microwave radiation at a preset temperature of 100 °C for 10 min. The carboxylated functionalization/ destruction of CNTs were carried out in the microwave accelerated reaction system by dispersing pre-weighed CNTs into a mixture of concentrated $H_2SO_4$ and $HNO_3$ (1:1 volume ratio) and treated at a preset temperature of 140 °C for 10, 20, 40, 60 and 120 min, respectively. In a typical treatment, 1 g CNTs was mixed with 40 ml of acid mixture. The resulting CNTs are referred to as $CNT_{10}$, $CNT_{20}$, $CNT_{40}$, $CNT_{60}$ and $CNT_{120}$, respectively. After cooling down to room temperature, the CNT products were vacuum filtered and washed using Milli Q water through pore size 10 μm until a neutral pH. Samples were then finally dried in a vacuum oven at 70 °C until a constant weight was achieved. The treated CNTs were also washed with 0.01M NaOH until the filtrate was clear. The filtrates contained debris and fragments washed off the main nanotube structures.

### 5.2.3 Materials Characterization

A scanning electron microscope (SEM, LEO 1530 VP, Carl Zeiss SMT Inc., Peabody, MA) equipped with an energy-dispersive X-ray analyzer (EDX, Oxford Instruments, Concord, MA) was used for morphology and elemental composition analysis. The CNT samples were dispersed in Milli Q water, added to 200-mesh TEM grids and dried. The transmission electron microscopy (TEM) was taken on a Hitachi H-7500 system. Raman spectroscopy was carried on a DXR Raman microscope (Thermo Fisher Scientific Inc., Madison, WI). The Brunauer, Emmett and Teller (BET) specific surface area of the samples were measured using Quantachrome NOVA 3000 series (Model N32-11) High

Speed Gas Sorption Analyzer at 77.40 K (Boynton Beach, FL). The Fourier transform infrared spectroscopy (FTIR) of CNT samples was done on a Perkin-Elmer instrument (Waltham, MA), with CNTs mixed with purified KBr and pressed into pellets. Cyclic voltammetry (CV) was carried out on a Homiangz 320C electrochemical analyzer versus a standard Ag-AgCl electrode in 2M $Na_2SO_4$ electrolyte. Galvanostatic charge – discharge measurements were carried out using a MTI Battery Analyzer (Richmond, CA) while energy, voltage and time were recorded.

## 5.3 Carboxylated and Defective Carbon Nanotubes for Supercapacitors

### 5.3.1 Characterization of the CNTs

The SEM images of the CNTs are shown in Figure 5.1. The microwave treatment led to significant tube damage and it can be seen that as the duration of microwave treatment was increased, the tubes were reduced in length. They also began to lose their individual long bundle structure and form gel like agglomerates, though their tubular structure remained intact (S. Addo Ntim, S. Mitra, 2012), (D. S. Ahmed et al., 2013). A typical microwave induced carboxylation can be achieved in 10 min (Y. Chen, S. Mitra, 2008), however, to generate defects the microwave treatments as long as 120 min were used in this study. The CNTs treated for 10, 20, 40, 60 and 120 min were referred as $CNT_{10}$, $CNT_{20}$, $CNT_{40}$, $CNT_{60}$ and $CNT_{120}$, respectively. The longer the treatment, more defective was their structure. The microwave treatment in acid introduced hydrophilic carboxylic groups (Y. Chen, S. Mitra, 2008) and (Z. Wu et al., 2014). However, once past a 40 min treatment time, there were less significant changes in morphology. The concentration of acids was also an important factor. While the dilute acids removed impurities, the concentrated acids introduced more defects (Y. Chen et al., 2007). The TEM images of the CNTs used in the

anode are shown in Figure 5.2. It could be seen that even when the CNTs were treated for longer periods, there was no significant change in diameter though some tubes appeared to get cut as shorter fragments were observed. Another observation from the TEM images is that the highly functionalized CNTs dispersed better and formed fewer agglomerates.

EDX analysis of the CNTs showed that the oxygen contents increased with treatment time due to increase in carboxylation [Figure 5.3 (a)]. However, beyond 40 min, the oxygen percentage showed relatively small increase. It is inferred that after 40 min the major part of the microwave energy went to the destruction of the CNT structures rather than generating more functional groups on the main tubes. The gross morphology also changed after the microwave treatment, and this is obvious from Figure 5.1 (g), where the electrode materials with original and treated CNTs are shown. The treated CNT had more of a gel structure compared to the original CNTs which were powdery. The increase in hydrophilicity with carboxylation also helped electrode preparation, where the hydrophilic CNTs were less likely to agglomerate and formed uniform dispersions that could be useful for preparing the paste for making the electrodes (K. Kordás et al., 2006)(Y. Zhou Y, L. Hu, G. Grüner, 2006).

The CNTs were also washed using 1M NaOH solution to remove oxidation debris after functionalization. Since the debris was on the CNTs surface, they were expected to alter the electrochemical behavior. The SEM analysis [Figure 5.1 (f)] showed small debris/CNT fragments were generated from over functionalization and breakdown of the tube structure.

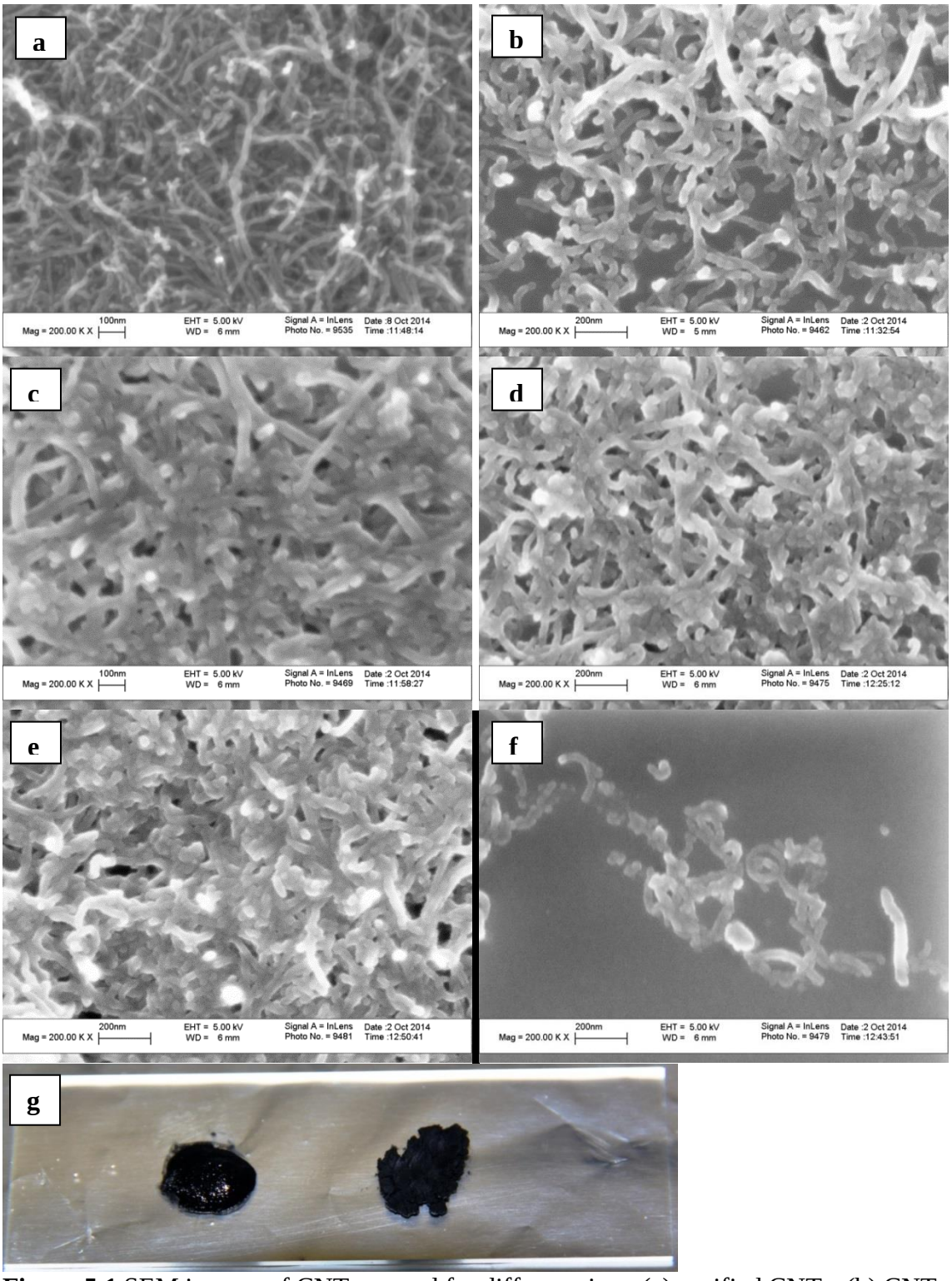


**Figure 5.1** SEM images of CNTs treated for different time: (a) purified CNTs; (b) $CNT_{20}$; (c) $CNT_{40}$; (d) $CNT_{60}$; (e) $CNT_{120}$; (f) debris created during treatment; and (g) electrode paste containing CNT60 (left) and purified CNTs (right).
*Source: Z. Wang et al., 2015*

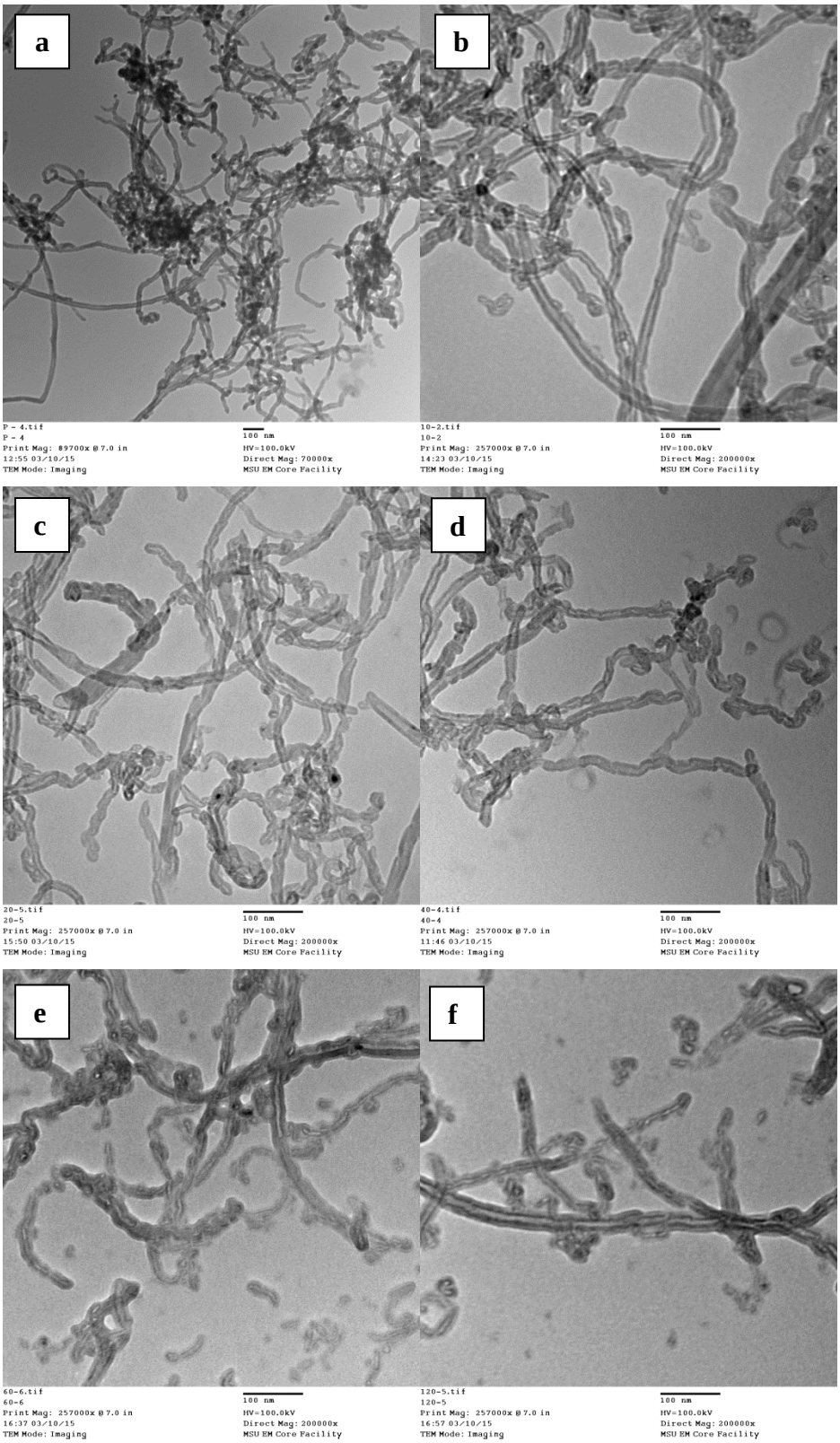


**Figure 5.2** TEM images of CNTs treated for different time: (a) purified CNTs; (b) $CNT_{10}$; (c) $CNT_{20}$; (d) $CNT_{40}$; (e) $CNT_{60}$; (f) $CNT_{120}$.
*Source: Z. Wang et al., 2015*

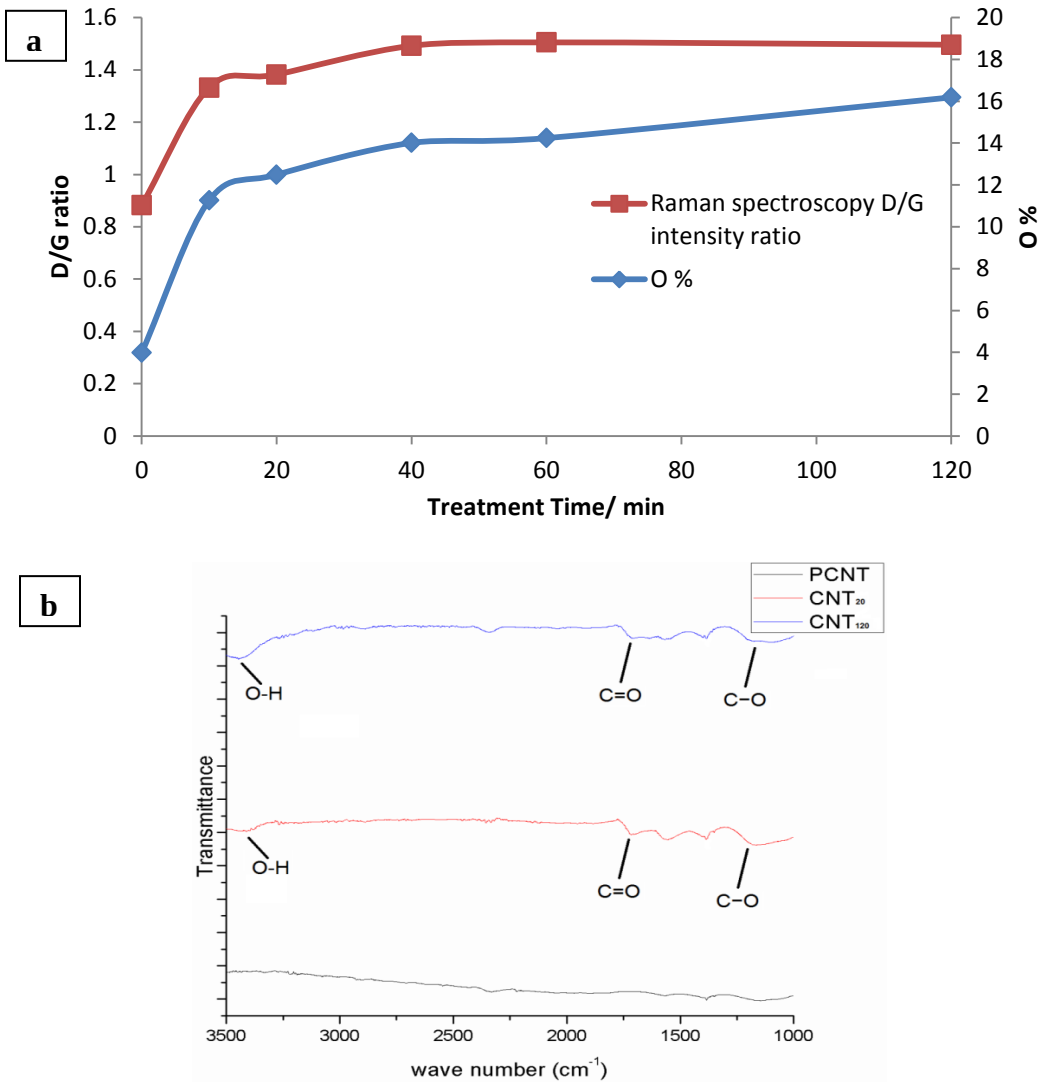


**Figure 5.3** Oxygen contents in CNTs after functionalization: (a) Weight percentage of oxygen in CNTs and D to G ratio of Raman spectra; (b) FTIR spectrum of purified CNT, $CNT_{20}$ and $CNT_{120}$.
*Source: Z. Wang et al., 2015*

EDX analysis showed that for the CNTs treated for 40 min or longer, the debris contained nearly 50% of oxygen by weight. Raman spectroscopy also confirmed the defect generation where the ratio of defect band (D band)/graphite band (G band) was studied [Figure 5.3 (a)]. The D to G ratio increased by more than 50% in the first 10 min of microwave treatment indicating that many of the defects and functional groups were

created at the beginning of the treatment. After that the increase was slower, indicating that the inner parts of the CNTs were much harder to destroy and react. However, D/G ratio continued to increase till 40 min of treatment.

Fourier transform infrared spectroscopy (FTIR) results of purified CNTs, $CNT_{20}$ and $CNT_{120}$ were shown in Figure 5.3 (b). Peaks indicating oxidative functional groups were observed for the functionalized CNTs. The newly generated peaks at around 1740 $cm^{-1}$ indicated the C=O stretching; while the peaks at 3300 $cm^{-1}$ indicated OH groups. Other peaks observed included C-O stretching at 1100 $cm^{-1}$, O-H bending at 1390 $cm^{-1}$ and C=C bending at 1580 $cm^{-1}$.

BET specific surface areas of the CNTs are shown in Table 5.1. Although nonporous, the CNTs have relatively large surface area and the surface area increased with the treatment time. This further showed that during the strong acid microwave treatment the specific area of CNTs increased but the most of it occurred in the early stage of the treatment. The surfaces of CNTs were damaged by acids/microwave energy, where carbon-carbon bonds were broke and carbon atoms were removed, leaving defects and openings that led to an increase in the surface area. After 40 min, the increase was slow and this was in line with the EDX and Raman measurements.

**Table 5.1** Characteristics of CNTs Treated for Different Time

| **Functionalization Time (min)** | **0 (purification)** | **10** | **20** | **40** | **60** | **120** |
|---|---|---|---|---|---|---|
| BET Specific surface area ($m^2 g^{-1}$) | 220.4 | 246.8 | 245.7 | 266.0 | 263.2 | 278.7 |
| Specific Capacitance ($F g^{-1}$) | 17.7 | 46.7 | 54.0 | 65.1 | 65.8 | 64.0 |
| Specific Energy for whole cell ($Wh kg^{-1}$) | 2.3 | 4.85 | 5.63 | 7.13 | 7.3 | 6.68 |

*Source: Z. Wang et al., 2015*

### 5.3.2 Electrochemical Tests: Cyclic Voltammetry

Cyclic voltammetry (CV) curves obtained versus a standard Ag-AgCl electrode is shown in Figure 5.4. At all scan rates the functionalized CNTs showed better performance than purified CNTs. Electrode currents increased from purified CNT till $CNT_{40}$ and $CNT_{60}$, after which the performance decreased. It is inferred that the performance drop was due to the defects which might block the electron migration and transfer, leading to an increase in CNT resistance. Under lower scan rates the difference among CNTs were more dramatic, indicating that highly functionalized CNTs with higher resistance would perform better when more time was allowed for electrons/charge to migrate to the nanotube surface so that the electric double layers could form. A comparison of $CNT_{120}$ and $CNT_{20}$ shows that under low scan rates (0.005 V/s) the former provided better performance, however, under high scan rates (0.1 V/s) the latter was better.

### 5.3.3 Charge/Discharge Characteristics: Asymmetric Supercapacitors

The capacitors were charged and discharged under constant current conditions. Figure 5.5 shows Galvanostatic charge/discharge curves measured at a current density of 0.1 A $g^{-1}$ electrode between 0 and 1.6 V with IR drops of approximately 0.06 V at the beginning of each discharge. No gas evolution was observed. Specific capacitance was calculated from the slopes of Galvanostatic charge–discharge curves (like the one shown in Figure 5.5, 11th cycle in our case) using the following equation (5.1):

$$Csp = \frac{I}{m \times dV/dt} \quad (5.1)$$

where I is the discharge current, m is the mass of CNTs and dV/dt is the slope of the linear part of the discharge curve, typically from 1.3 V to 0.6 V. This was calculated using linear least square fit. The results are also shown in Table 5.1. It showed that the specific

capacitance firstly increased as treatment time increased, with little improvement past 40 min of treatment time. The cell specific energy for functionalized CNTs after 100th cycles showed values between 10 and 17 Wh $kg^{-1}$ as shown in Table 5.1. Similar trend was observed for the measured cell capacities through the battery analyzer (Figure 5.6). The defects on the CNTs led to higher capacity. The purified CNT showed the lowest capacitance, while higher capacitances were obtained for $CNT_{10}$, $CNT_{20}$ and higher. The increase past $CNT_{40}$ were not significant which was similar for $CNT_{60}$ and $CNT_{120}$.

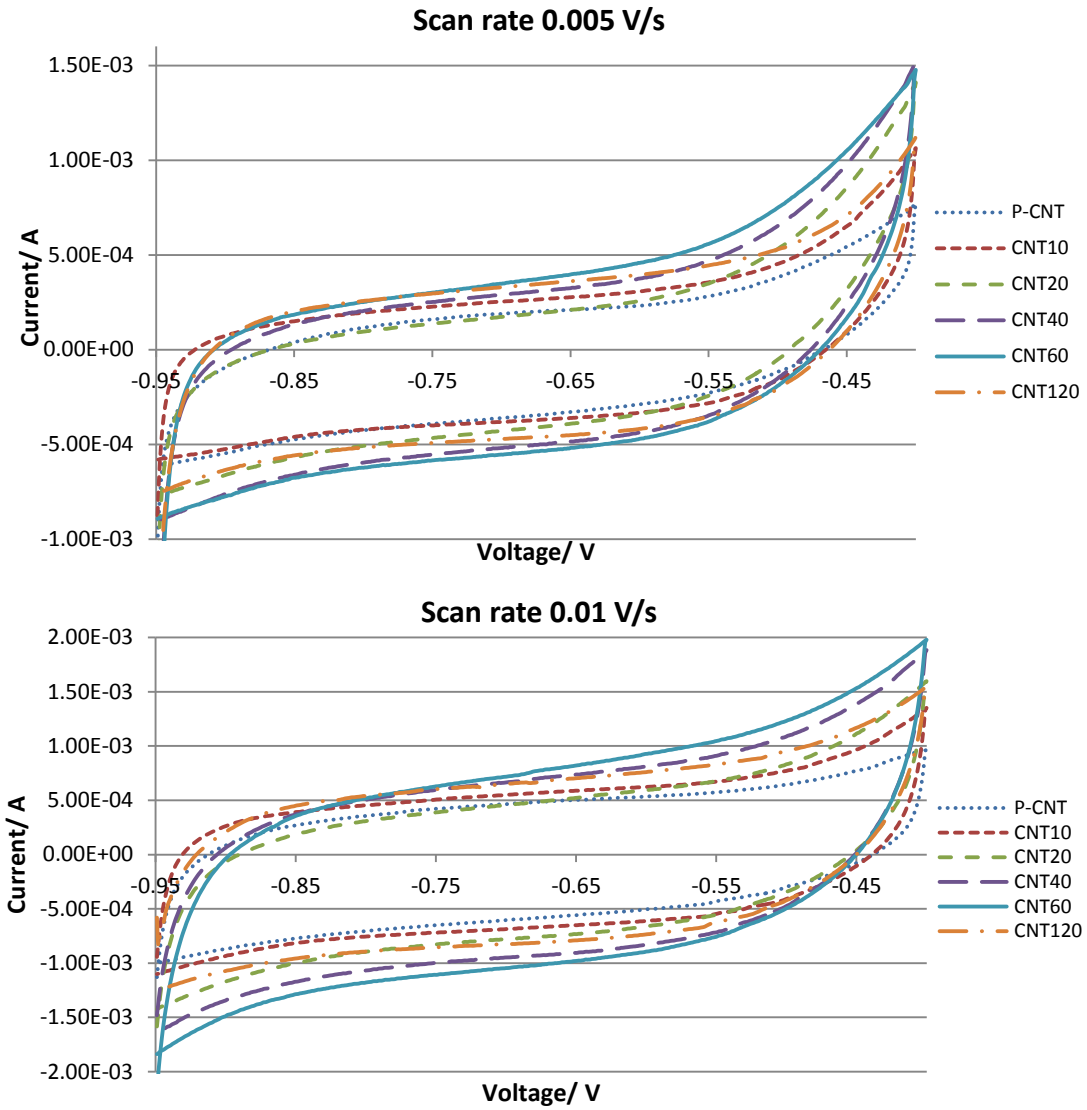


**Figure 5.4** Cyclic voltammetry (CV) curves under different scan rates.
*Source: Z. Wang et al., 2015*

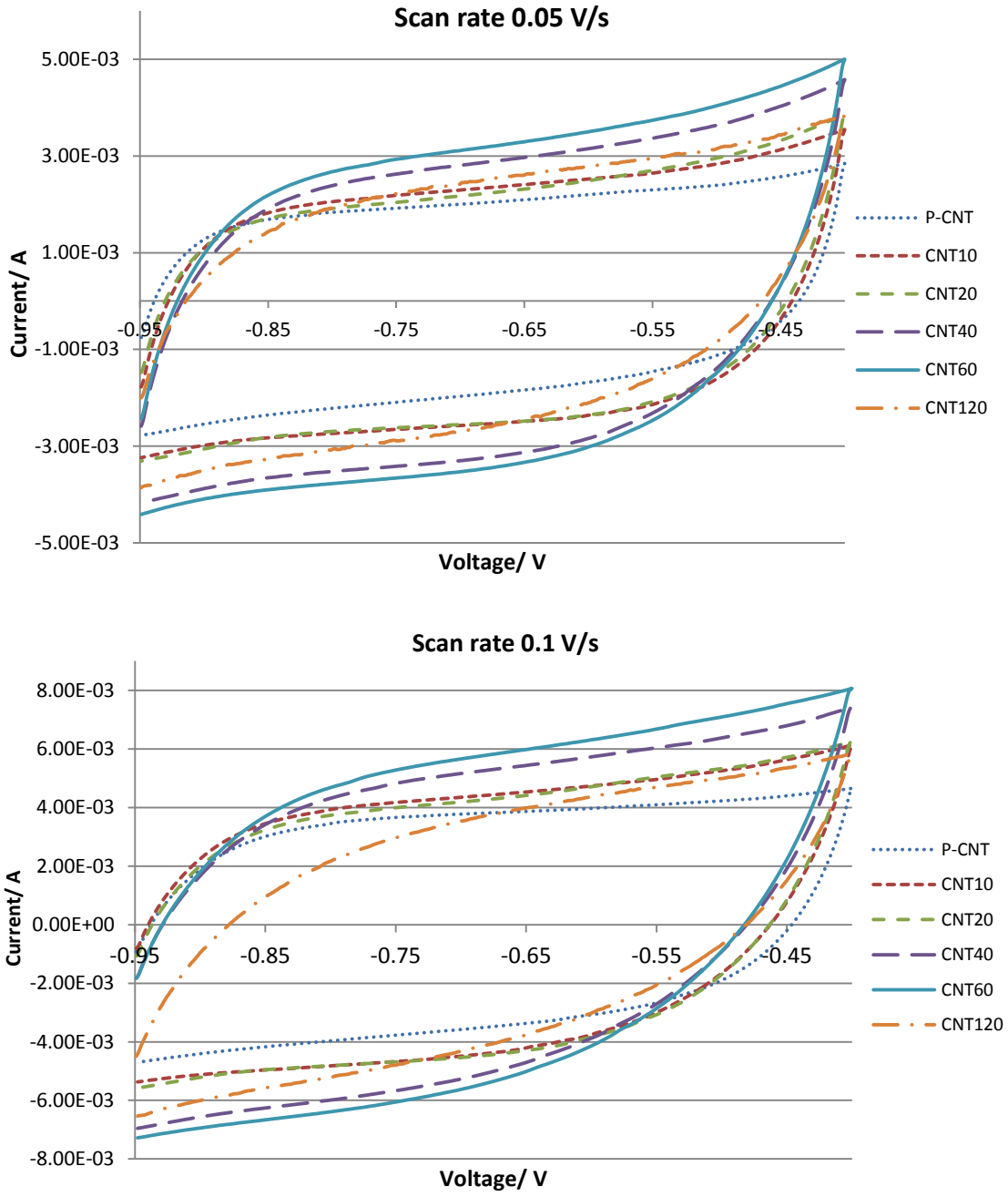


**Figure 5.4** Cyclic voltammetry (CV) curves under different scan rates (continued).
*Source: Z. Wang et al., 2015*

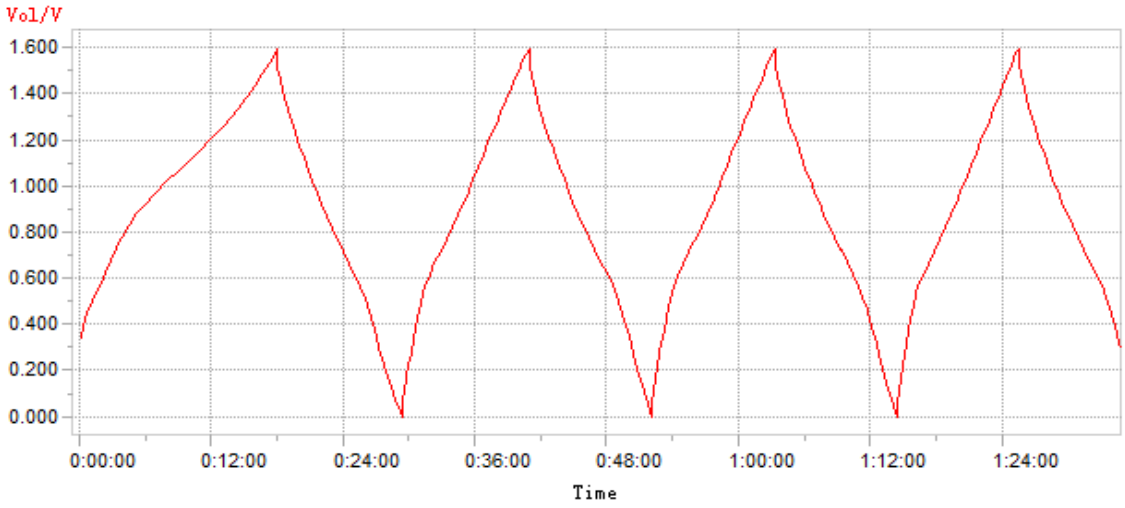


**Figure 5.5** Galvanostatic charge/discharge curves of an asymmetric supercapacitor (made from $CNT_{20}$).
*Source: Z. Wang et al., 2015*

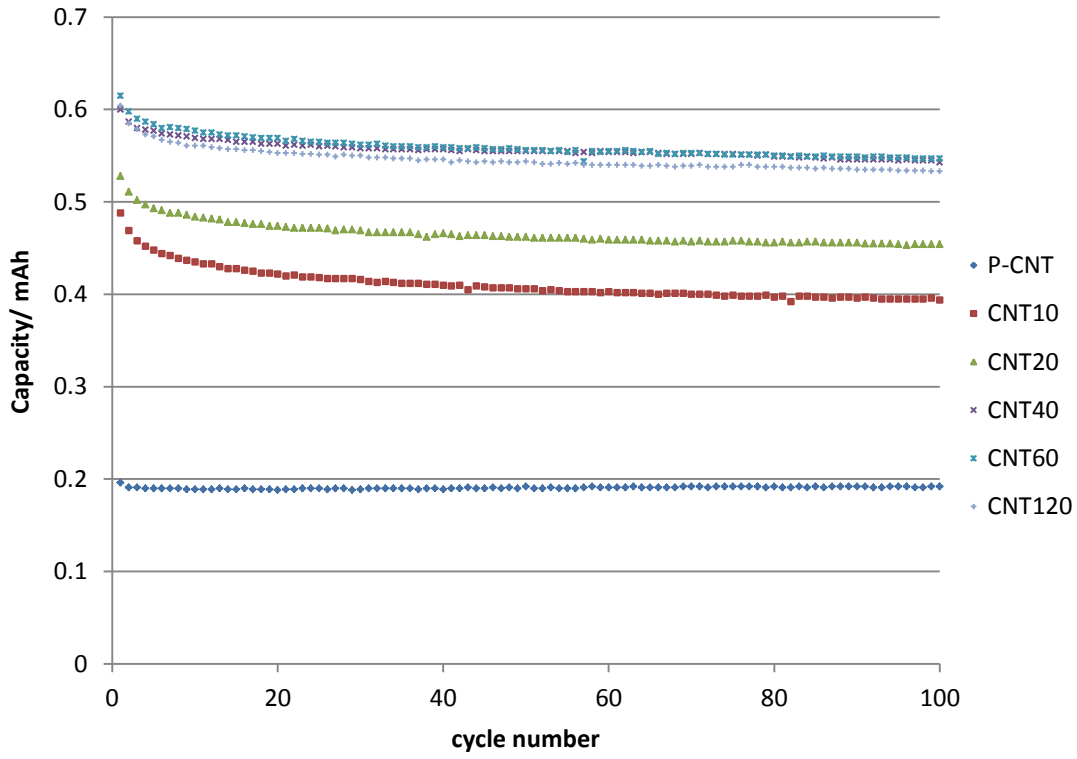


**Figure 5.6** Measured capacity of asymmetric cells at 0.1 A/g electrode.
*Source: Z. Wang et al., 2015*

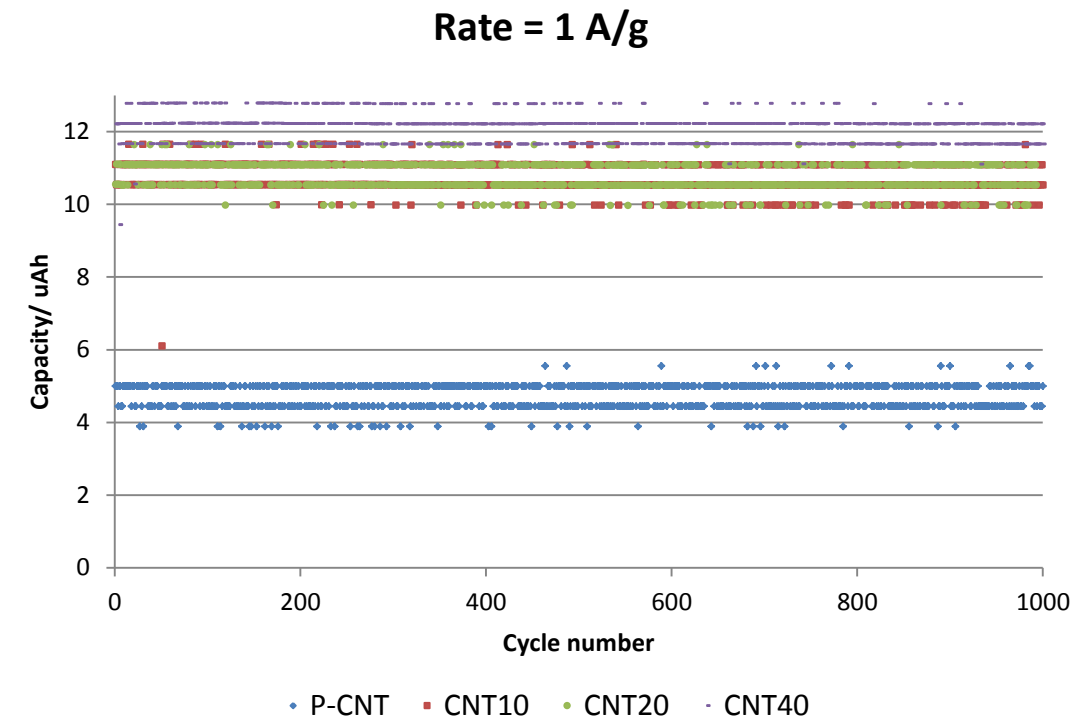


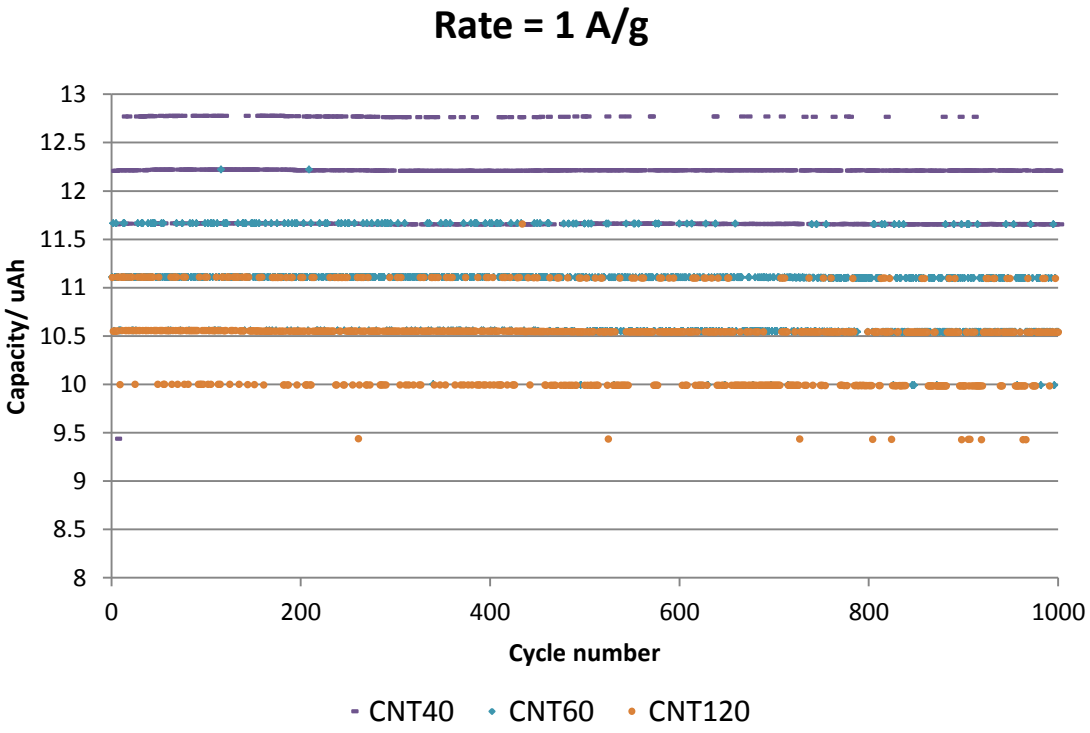


**Figure 5.7** Measured capacity of symmetric cells under different charge/discharge rates (P-CNT: dark blue; $CNT_{10}$: red; $CNT_{20}$: green; $CNT_{40}$: purple; $CNT_{60}$: light blue; $CNT_{120}$: orange).
*Source: Z. Wang et al., 2015*

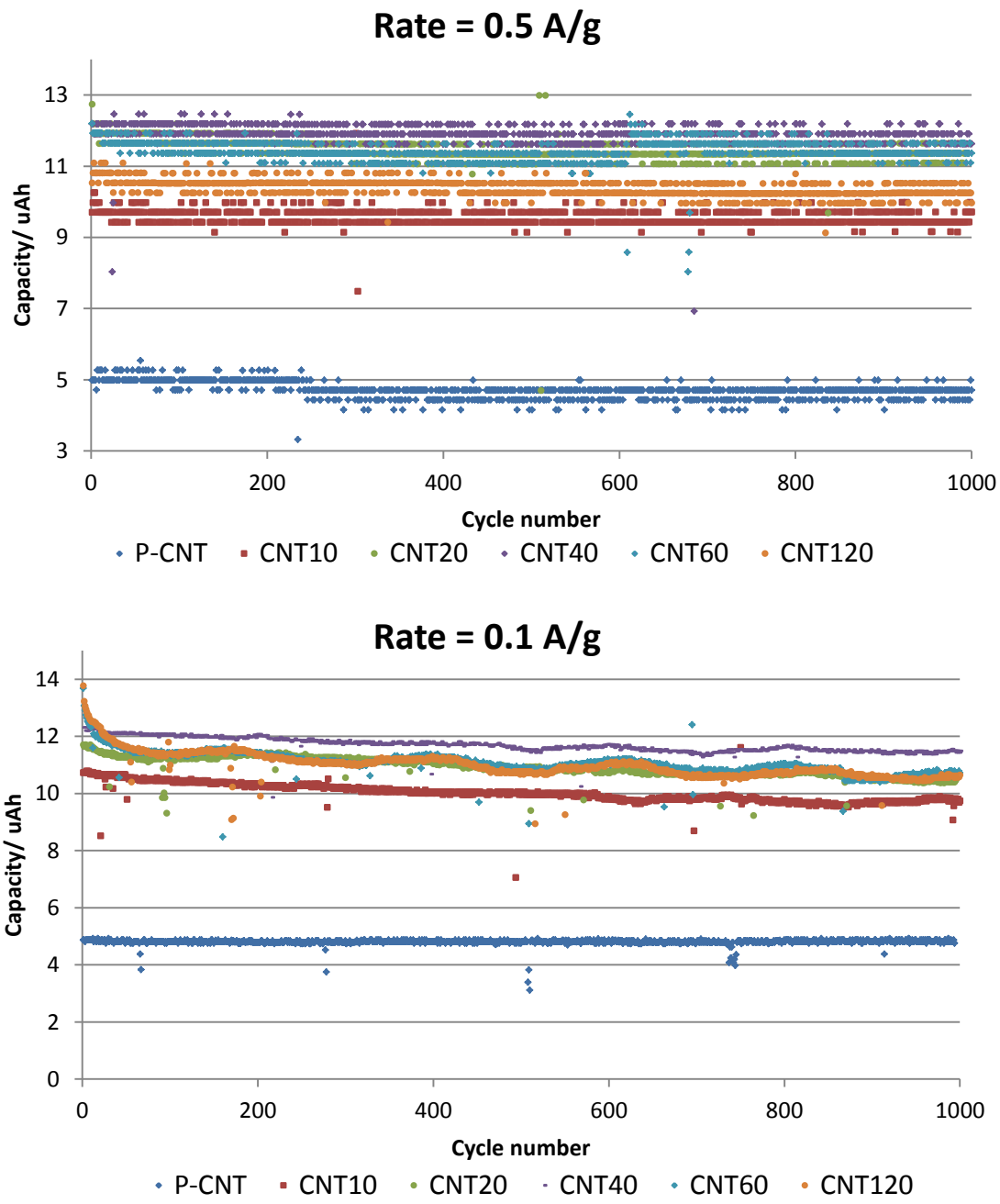


**Figure 5.7** Measured capacity of symmetric cells under different charge/discharge rates (P-CNT: dark blue; $CNT_{10}$: red; $CNT_{20}$: green; $CNT_{40}$: purple; $CNT_{60}$: light blue; $CNT_{120}$: orange), (continued).
*Source: Z. Wang et al., 2015*

### 5.3.4 Charge/Discharge Characteristics: Symmetric Supercapacitors

Figure 5.7 shows cycling characteristics of symmetric supercapacitors in which both electrodes were composed of CNTs. In all cases the functionalized CNTs provided higher performance than purified CNTs. In particular the moderately treated $CNT_{40}$ provided better performance. Beyond this the degree of functionalization did not enhance performance. One thing to note is that as the charge/discharge rate decreased, the difference between the CNT forms became more significant. Longer treated CNTs performed better under lower charge/discharge rates. For example, at 1 A/g $CNT_{120}$ showed similar capacity as $CNT_{10}$, however, at 0.5 A/g $CNT_{120}$ performed better. The difference was even more obvious at 0.1 A/g. The capacity of the cells was well retained and it was especially true for the moderately treated CNTs (95% after 1000 cycles). Under different charge/discharge rates, most of the functionalized CNTs also showed similar performance, though some highly treated CNTs (like $CNT_{120}$) tended to perform better at lower rates.

The mechanism underlying the CNT electrode is the double-layer capacitance in which the available specific area is a critical parameter. The microwave treatment created defects and increased the sites for ions and surface area for charge. At the same time the tips of CNTs were cut off, thus allowing the ions to penetrate inside [Figure 5.8 (a)]. With the tube tips cut off and surface defected, the open structure enabled easy access of ions to the electrode/electrolyte interface, which is critical for charging the electrical double layer. Another consideration is that although the CNTs themselves showed high specific area, during the fabrication of the electrodes the CNTs might agglomerate to reducing the effective surface area. In aqueous environment, the added functional groups in the

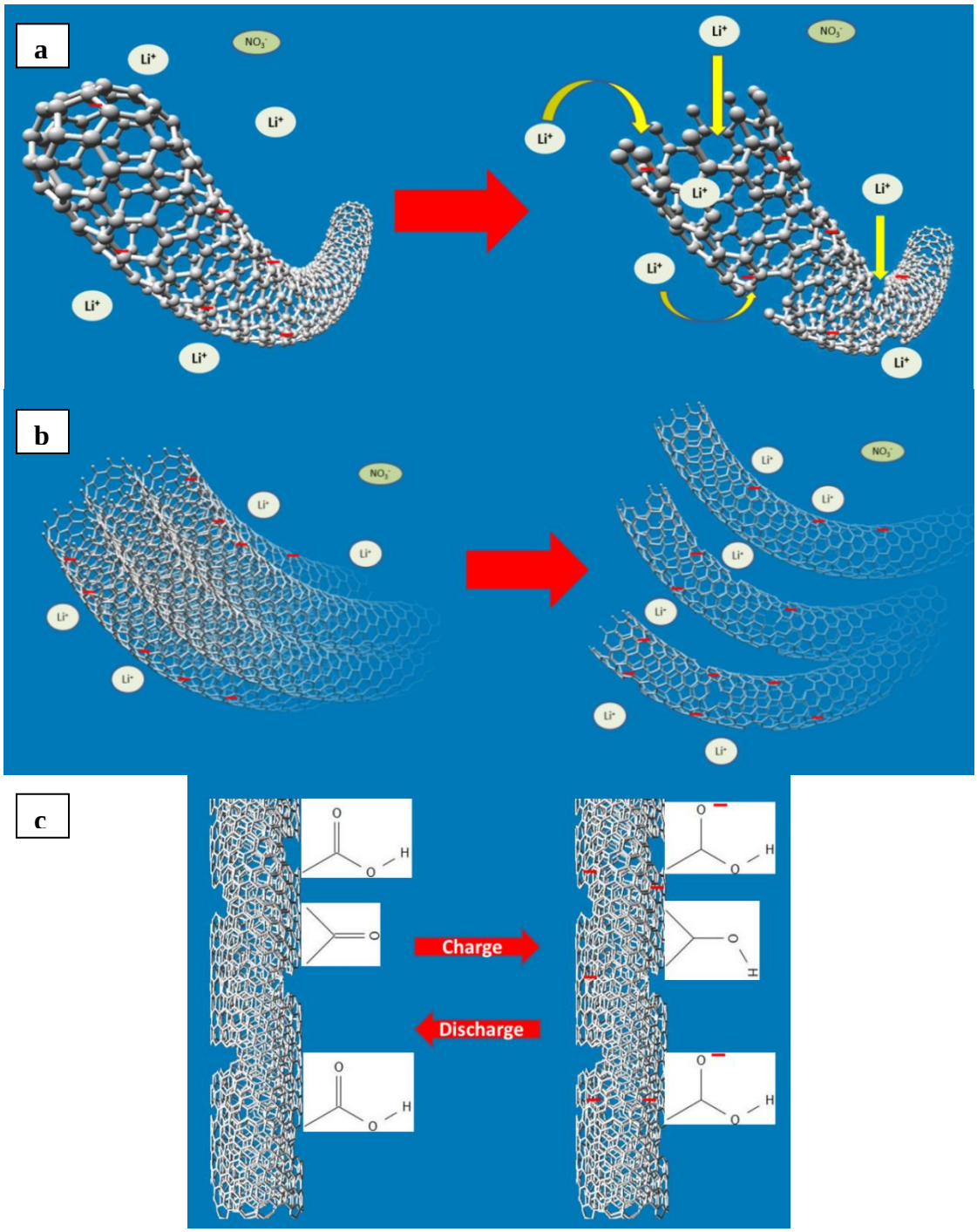


**Figure 5.8** CNTs before (left) and after (right) microwave treatment: (a) creation of defects and removal of CNT tips; (b) functionalized CNTs separate from each other in electrolyte, generating more surface area; (c) pseudocapacitance from oxygenated functional groups.
*Source: Z. Wang et al., 2015*

carboxylated CNTs reduced aggregation of the individual tubes, thus increasing the effective surface area. This explains the fact that in spite of BET surface area, CNTs tend to aggregate, decreasing the effective surface area; while CNTs with more carboxylic groups would remain separate from each other [Figure 5.8 (b)]. While the major mechanism is double-layer capacitance in our case, it has also been reported that pseudocapacitance could be brought about by the function groups [Figure 5.8 (c)] via reversible oxidation of OH groups into C=O groups and reduction of C=O groups into $C\text{-}O^-$ according to: (E. Frackowiak et al., 2000)

$$C\text{-}OH \leftrightarrow C{=}O + H^+ + e^-$$

$$C{=}O + e^- \leftrightarrow C\text{-}O^-$$

Past the 40 min of treatment, the increase in oxygen contents was not that significant; consequently there was no significant increase in specific capacitance. This also demonstrated pseudocapacitance associated with the oxidative functional groups like carboxylic groups in some cases. This was consistent with previous reports E. Frackowiak et al., 2000).

## 5.4 Conclusions

In summary, the microwave treatment for generating defective CNTs for supercapacitor applications that has several advantages has been studied. The increase in treatment time created more defects and oxygen containing carboxylic groups. Also, there were changes to the CNT structures where the longer tubes were shortened and bundles were separated during the treatment. Carboxylic groups also prevented CNT aggregation. Together, these led to higher effective specific surface area which increased the specific capacitance. Hence, the microwave treatment of CNTs for supercapacitors electrodes has the potential

of further increasing the capacitance via the double layer capacitance and pseudocapacitance, making the defective CNTs promising candidates for supercapacitors. There have also been reports where metal oxides were coated on the CNTs to form supercapacitor electrodes (R. K. Sharma, L. Zhai, 2009). The functionalized approach is also promising in preparing CNTs as the scaffolds or matrix for the metal oxides to further enhancing the capacitance. The functional groups and hydrophilicity also facilitate the formation of inks/ pastes for electrode preparation, hence, facilitating the development of flexible electrodes via printing techniques (P. Chen et al., 2010), (M. Kaempgen et al., 2009).

# CHAPTER 6

# CONCLUSIONS

In summary, a technological platform for flexible battery fabrication was built. Flexible zinc carbon battery, primary and secondary alkaline batteries were developed and optimized. Carbon nanotubes are treated with acids and microwave energy heavily to generate large amount of defects and then used as supercapacitor electrodes. Preliminary studies on flexible zinc air battery were also taken. The development and application of nanomaterials, polymers and printing techniques has make the fabrication of flexible power sources possible, providing decent performance for nowadays and future flexible electronics. Nano-carbons act as conductive additives, current collectors, scaffolds for active materials or major electrode materials themselves, behaving much more efficiently than the traditional materials like graphite; while further certain treatment like purification further enhanced the electrochemical performance by removing impurities which might facilitate self-discharge or other unwanted electrode (especially zinc) corrosions and side reactions. Treatments that added functional groups or change surface morphologies had also been proved helpful regarding changes in hydrophobicity, dispersibility, surface areas and electrochemical properties, which might enhance the electrochemical performance of power sources. Polymers served as separators, binders, gel electrolytes or even conductive additives, acquiring the desired flexibility and kept the electrochemical devices functional under bending conditions. This platform can be used to fabricate different types of flexible power sources include but not limited to the types of flexible batteries mentioned in the former chapters. Flexible supercapacitors can also be fabricated in similar ways.

## REFERENCES


T Reddy, Linden's Handbook of Batteries, 4th Edition 2010.

J. C. Bailey, A. Hilmi, M. A. Schubert, J. Zhang, G. Zheng, US Patent Application 20100209756 A1 (2010).

G. R. Tucholski, US Patent Application 20110311857 A1 (2011).

D. Southee, G. Hay, P. Evans, D. Harrison, Circuit World 33 (2007) 31.

Y.G. Lee, M. G. Choi, K. Y. Kang, K. M. Kim, J. Electrochem. Sci. and Tech. 1 (2010) 39.

M. Choi, K. M. Kim, Y. G. Lee, Curr. Appl. Phys. 10 (2010) e92.

G. Wang, Q. Zhang, Z. Yu, M. Qu, Solid State Ionics 179 (2008) 263.

Y. Feng, Mat. Chem. Phys. 121 (2010) 302.

Y. J. Kim, Y. A. Kim, T. Chino, H. Suezaki, M. Endo, M. S. Dresselhaus, Small 2 (2006) 339.

G. Wang, Z. Shao, Z. Yu, Nanotechnology 18 (2007) 205705.

C. Meng, C. Liu, S. Fan, Electrochem. Commun. 11 (2009) 186.

X. Jia, C. Yan, Z. Chen, R. Wang, Q. Zhang, L. Guo, F. Wei, Y. Lu, Chem. Commun. 47 (2011) 9669-9671.

L. Hu, H. Wu, F. La Mantia, Y. Yang, Y. Cul, ACS Nano 4 (2010) 5843-5848.

A. Kiebele, G. Gruner, Appl. Phys. Lett. 91 (2007) 144104.

P. Hiralal, S. Imaizumi, H. E. Unalan, H. Matsumoto, M. Minagawa, M. Rouvala, A. Tanioka, G. Amaratunga, ACS Nano 4 (2010) 2730-2734.

Y. H. Kim, C. Sachse, M. Machala, C. May, L. Mueller-Meskamp, K. Leo, Adv. Func. Mat. 21 (2011) 1076.

C. Lei, P. Wilson, C. Lekakou, J. Power Sources, 196 (2011) 7823.

A. Laforgue, J. Power Sources 196 (2011) 559.

R. K. Sharma and L. Zhai, Electrochimica. Acta 54 (2009) 7148-7155.

Y. Chen, Z. Iqbal and S. Mitra, Adv. Funct. Mater. 17 (2007) 3946-3951.

C. Ionescu-Zanetti, A. Mechler, S. A. Carter, R. Lal, Adv. Mat. 16 (2004) 385.

Z. Hu, J. Zhang, Z. Hao, Y. Zhao, Solar Energy Materials & Solar Cells 95 (2011) 2763

Y. Kim, J. Lee, H. Kang, G. Kim, N. Kim, K. Lee, Solar Energy Materials & Solar Cells 98 (2012) 39.

T.W. Chou, L. Gao, E. Thostenson, Z. Zhang, J. H. Byun, Comp. Sci. Tech. 70 (2010) 1

Y. Liu, L. Gao, Carbon 43 (2005) 47.

Z. Spytalsky, C. Krontiras, S. Georga, C. Gallotis, Composites Part A: Appl. Sci. and Manufact. 40 (2009) 778-783.

Q. Li, Y. Li, X. Zhang, S. Chikkannanavar, Y. Zhao, A. Dangelewicz, L. Zheng, S. Doorn, Q. Jia, D. Peterson, P. Arendt, Y. Zhu, Adv. Mater. 19 (2007) 3358-3363

Z. Wang, N. Bramnik, S. Roy, G. D. Benedetto, J. L. Zunino III and S. Mitra, J. Power Sources 237 (2013) 210-214.

A. M. Gaikwad, G. L. Whiting, D. A. Steingart, A. C. Arias, Adv. Mat. 23 (2011) 3251-3255.

Y. C. Chen, Y. K. Hsu, Y. G. Lin, Y. K. Lin, Y. Y. Horng, L. C. Chen, K. H. Chen, Electrochim. Acta 56 (2011) 7124-7130.

A. M. Gaikwad, J. W. Gallaway, D. Desai, D. A. Steingart, J. Electrochem. Soc. 158 (2011) A154

A. M. Gaikwad, D. A. Steingart, T. N. Ng, D. E. Schwartz, Appl. Phys. Lett. 102 (2013) 233302.

L. Bao, J. Zang, X. Li, Nano Lett. 11 (2011) 1215-1220.

L. Bao, X. Li, Adv. Mater. 24 (2012) 3246-3252.

Y. Zhang, T. Chen, J. Wang, G. Min, L. Pan, Z. Song, Z. Sun, W. Zhou, J. Zhang, Appl. Surf. Sci. 258 (2012) 4729-4732.

K. Kumeta, I. Nagashima, S. Matsui, K. Mizoguchi, J. Appl. Polym. Sci. 90 (2003) 2420-2427.

J. Zang, X. Li, J. Mater. Chem. 21 (2011) 10965-10969.

A. A. Mohamad, N. S. Mohamed, M. Z. A. Yahya, R. Othman, S. Ramesh, Y. Alias, A. K. Arof, Solid State Ion. 156 (2003) 171-177.

G. M. Wu, S. J. Lin, C. C. Yang, J. Membr. Sci. 275 (2006) 127-133.

H. H. Wang, T. W. Shyr, M. S. Hu, J. Appl. Polym. Sci. 74 (1999) 3046-3052.

X. Zhang, Y. Cui, Z. Lv, M. Li, S. Ma, Z. Cui, Q. Kong, Int. J. Electrochem. Sci. 6 (2011) 6063-6073.

G. Mpourmpakis, E. Tylianakis, D. Papanikolaou, G. Froudakis, Rev. Adv. Mater. Sci. 11 (2006) 92-97.

G. W. Gokel, S. L. De Wall, E. S. Meadows, Eur. J. Org. Chem. (2000) 2967-2978.

F. Valentini, A. Amine, S. Orlanducci, M.L. Terranova, G. Palleschi, Anal. Chem. 75 (2003) 5413-5421.

Y. Liu, L. Gao, Carbon 43 (2005) 47-52.

V. Ravindran, V.S. Muralidharan, J. Power Sources 55 (1995) 237-241.

A. R. Suresh Kannan, S. Muralidharan, K. B. Sarangapani, V. Balaramachandran, V. Kapali, J. Power Sources 57 (1995) 93-98.

J. Y. Huot, E. Boubour, J. Power Sources 65 (1997) 81-85.

J. Dobryszyckia, S. Biallozor, Corros. Sci. 43 (2001) 1309-1319.

M. J. Hey, D. P. Jackson, H. Yan, Polymer 46 (2005) 2567-2572.

Y. Chen, S. Mitra, J. Nanosci. Nanotechnol. 8 (2008) 5770-5775.

J. P. Coleman, A.T. Lynch, P. Madhukar, J.H. Wagenknecht, Sol. Energ. Mat. Sol. C 56 (1999) 395-418.

R. Hahn, H. Reichl, in: Wearable Computers, 1999. Digest of Papers. The Third International Symposium on, 1999, pp. 168-169.

A. C. Siegel, S.T. Phillips, M.D. Dickey, N. Lu, Z. Suo, G.M. Whitesides, Adv. Funct. Mater. 20 (2010) 28-35.

K. Gao, Z. Shao, J. Li, X. Wang, X. Peng, W. Wang, F. Wang, Journal of Materials Chemistry A, 1 (2013) 63-67.

Y. Zhao, Q. Zhou, L. Liu, J. Xu, M. Yan, Z. Jiang, Electrochim Acta, 51 (2006) 2639-2645.

N. A. Hamid, S. Wennig, S. Hardt, A. Heinzel, C. Schulz, H. Wiggers, J. Power Sources, 216 (2012) 76-83.

J. F. Ihlefeld, P.G. Clem, B.L. Doyle, P.G. Kotula, K.R. Fenton, C.A. Apblett, Adv. Mater. 23 (2011) 5663-5667.

L. Noerochim, J. Z. Wang, S. L. Chou, D. Wexler, H. K. Liu, Carbon 50 (2012) 1289-1297.

H. M. Ren, Y. H. Ding, F. H. Chang, X. He, J. Q. Feng, C. F. Wang, Y. Jiang, P. Zhang, Appl. Surf. Sci. 263 (2012) 54-57.

J. Saunier, F. Alloin, J.Y. Sanchez, G. Caillon, J. Power Sources 119-121 (2003) 454-459.

F. Beck, P. Rüetschi, Electrochim Acta 45 (2000) 2467-2482.

Y. Shen, K. Kordesch, J. Power Sources 87 (2000) 162-166.

M. Ghaemi, R. Amrollahi, F. Ataherian, M.Z. Kassaee, J. Power Sources 117 (2003) 233-241.

X. C. Lau, C. Desai, S. Mitra, Sol. Energy 91 (2013) 204-211.

G. Dennler, S. Bereznev, D. Fichou, K. Holl, D. Ilic, R. Koeppe, M. Krebs, A. Labouret, C. Lungenschmied, A. Marchenko, D. Meissner, E. Mellikov, J. Méot, A. Meyer, T. Meyer, H. Neugebauer, A. Öpik, N.S. Sariciftci, S. Taillemite, T. Wöhrle, Sol. Energy 81 (2007) 947-957.

X. C. Lau, Z. Wang, S. Mitra, Appl. Phys. Lett. 103 (2013) 243108.

P. Arora, Z. Zhang, Chem. Rev. 104 (2004) 4419-4462.

Z. Wang, Z. Wu, N. Bramnik, S. Mitra, Adv. Mater. 26 (2014) 970-976.

B. J. Landi, M. J. Ganter, C. D. Cress, R. A. DiLeo, R. P. Raffaelle, Energy & Environmental Science 2 (2009) 638-654.

S. L. Candelaria, Y. Shao, W. Zhou, X. Li, J. Xiao, J. G. Zhang, Y. Wang, J. Liu, J. Li, G. Cao, Nano Energy 1 (2012) 195-220.

Z. Wang, S. Mitra, J. Power Sources 266 (2014) 296-303.

A. Stani, W. Taucher-Mautner, K. Kordesch, J. Daniel-Ivad, J. Power Sources 153 (2006) 405-412.

R. Shivkumar, G. Paruthimal Kalaignan, T. Vasudevan, J. Power Sources 55 (1995) 53-62.

M. Minakshi, M. Blackford, M. Ionescu, J. Alloy Compd. 509 (2011) 5974-5980.

C. Cachet, Z. Chami, R. Wiart, Electrochim Acta 32 (1987) 465-474.

C. Cachet, B. Saïdani, R. Wiart, Electrochim Acta, 33 (1988) 405-416.

C. Cachet, B. Saïdani, R. Wiart, Electrochim Acta, 34 (1989) 1249-1250.

F. Y. Cheng, J. Chen, X. L. Gou, P. W. Shen, Adv. Mater. 17 (2005) 2753-2756.

P. Simon, Y. Gogotsi, Nat Mater, 7 (2008) 845-854.

J. R. Miller, P. Simon, Science, 321 (2008) 651-652.

V. V. N. Obreja, Physica E: Low-dimensional Systems and Nanostructures, 40 (2008) 2596-2605.

B. E. Conway, V. Birss, J. Wojtowicz, J Power Sources, 66 (1997) 1-14.

Y. Zhang, H. Feng, X. Wu, L. Wang, A. Zhang, T. Xia, H. Dong, X. Li, L. Zhang, International Journal of Hydrogen Energy, 34 (2009) 4889-4899.

L. Y. Chen, Y. Hou, J. L. Kang, A. Hirata, T. Fujita, M. W. Chen, Adv Energy Mater, 3 (2013) 851-856.

J. Jiang, Y. Li, J. Liu, X. Huang, C. Yuan, X.W. Lou, Adv Mater, 24 (2012) 5166-5180.

G. Wang, L. Zhang, J. Zhang, Chemical Society Reviews, 41 (2012) 797-828.

L. T. Le, M. H. Ervin, H. Qiu, B. E. Fuchs, W. Y. Lee, Electrochemistry Communications, 13 (2011) 355-358.

M. Zhi, C. Xiang, J. Li, M. Li, N. Wu, Nanoscale, 5 (2013) 72-88.

E. Frackowiak, F. Béguin, Carbon, 39 (2001) 937-950.

E. Frackowiak, K. Jurewicz, S. Delpeux, F. Béguin, Journal of Power Sources, 97-98 (2001) 822-825.

E. Frackowiak, K. Méténier, R. Pellenq, S. Bonnamy, F. Béguin, AIP Conference Proceedings, 486 (1999) 429-432.

M. Manickam, P. Singh, T.B. Issa, S. Thurgate, R. De Marco, J Power Sources, 130 (2004) 254-259.

Y. Wang, J. Yi, Y. Xia, Adv Energy Mater, 2 (2012) 830-840.

Y. G. Wang, Y. Y. Xia, Electrochemistry Communications, 7 (2005) 1138-1142.

C. G. Salzmann, S. A. Llewellyn, G. Tobias, M. A. H. Ward, Y. Huh, M. L. H. Green, Adv Mater, 19 (2007) 883-887.

F. Hauke, A. Hirsch, Covalent Functionalization of Carbon Nanotubes, in: Carbon Nanotubes and Related Structures, Wiley-VCH Verlag GmbH & Co. KGaA, 2010, pp. 135-198.

A. Stein, Z. Wang, M. A. Fierke, Adv Mater, 21 (2009) 265-293.

W. Huang, Y. Lin, S. Taylor, J. Gaillard, A.M. Rao, Y.-P. Sun, Nano Letters, 2 (2002) 231-234.

E. Frackowiak, K. Metenier, V. Bertagna, F. Beguin, Applied Physics Letters, 77 (2000) 2421-2423.

S. Addo Ntim, S. Mitra, Journal of Colloid and Interface Science, 375 (2012) 154-159.

D. S. Ahmed, A. J. Haider, M. R. Mohammad, Energy Procedia, 36 (2013) 1111-1118.

Z. Wu, R. F. Hamilton Jr, Z. Wang, A. Holian, S. Mitra, Carbon, 68 (2014) 678-686.

K. Kordás, T. Mustonen, G. Tóth, H. Jantunen, M. Lajunen, C. Soldano, S. Talapatra, S. Kar, R. Vajtai, P.M. Ajayan, Small, 2 (2006) 1021-1025.

Y. Zhou, L. Hu, G. Grüner, Applied Physics Letters, 88 (2006) 233302.

Y. J. Kang, B. Kim, H. Chung, W. Kim, Synthetic Metals, 160 (2010) 2510-2514.

R. K. Sharma, L. Zhai, Electrochimica Acta, 54 (2009) 7148-7155.

P. Chen, H. Chen, J. Qiu, C. Zhou, Nano Res., 3 (2010) 594-603.

M. Kaempgen, C.K. Chan, J. Ma, Y. Cui, G. Gruner, Nano Letters, 9 (2009) 1872-1876.

Z. Wang, Z. Wu, G. D. Benedetto, J. L. Zunino III, S. Mitra, Carbon (2015) doi: 10.1016/j.carbon.2015.04.045.